DISSERTATION

CLIMATE CONTROLS ON ECOSYSTEM-ATMOSPHERE CARBON EXCHANGE AND HYDROLOGICAL DYNAMICS IN ROCKY MOUNTAIN FENS

Submitted by

David Millar

Graduate Degree Program in Ecology

In partial fulfillment of the requirements

For the Degree of Doctor of Philosophy

Colorado State University

Fort Collins, Colorado

Spring 2015

Doctoral Committee:

Advisor: David Cooper

Kate Dwire
Robert Hubbard
Michael Ronayne
Joseph von Fischer

ABSTRACT

CLIMATE CONTROLS ON ECOSYSTEM-ATMOSPHERE CARBON EXCHANGE AND HYDROLOGICAL DYNAMICS IN ROCKY MOUNTAIN FENS

Groundwater fed peatlands known as fens are among the most important ecosystems in the Rocky Mountains of North America. These wetlands have sequestered atmospheric carbon dioxide for several millennia, provide important habitat for wildlife, and serve as refugia for regionally-rare plant species typically found in boreal regions. Perennially high water tables are critical for ecosystem functioning in fens, and provide conditions that support the development and persistence of organic soils. It is unclear how Rocky Mountain fens will respond to a changing climate, and those found at lower elevations may be particularly susceptible, where changes in hydrological cycles that control water tables are likely to be greatest. Further, it is unclear how regionally variable monsoon rainfall influences water tables and carbon dynamics, late in the growing season. In this dissertation I addressed the following questions: 1) How does ecosystem-atmosphere CO_2 exchange vary with elevation and monsoon influence in Rocky Mountain fens? 2) How do snowmelt dynamics at high and low elevations and varying monsoon influence affect groundwater dynamics in fens of the Rocky Mountains? 3) How will mountain fen hydrological dynamics potentially change under a future climate, and what will be the subsequent impact on ecosystem-atmosphere C exchange? My results show that net ecosystem production was higher for fens located at high elevations compared to those found at lower elevations. This was reflected in the negative correlation of growing season net ecosystem production with air temperature, and positive correlation with water table position, as the high

elevation sites had the lowest air temperatures and highest water tables. Study fens in the San Juan Mountains of southwest Colorado received almost twice as much late summer precipitation than those in the Medicine Bow Mountains of Wyoming, causing more frequent water table rises. However, differences in net ecosystem production associated directly with varying monsoon influence were less discernable. Peak snow water equivalent was lower for fens located at low elevations, and the snow-free season occurred approximately one month earlier at these sites compared to high elevation fens. The earlier onset of snow-free conditions led to steady declines in water table position early in the growing season at the low elevation fens, driven primarily by evapotranspiration. Under two future climate modeling scenarios at a low elevation fen, warmer air temperatures increased the proportions of winter precipitation that fell as rain, and peak snow water equivalent was reduced along with the number of days which snowpack persisted. Results from a coupled carbon exchange and hydrological model showed these changes in hydrological processes led to lower water tables that persisted through the growing season, and subsequently impacted ecosystem-atmosphere C exchange. Under the future climate scenarios, the overall global warming potential of gaseous C emissions increased as a result of increased ecosystem respiration, despite decreases in methane emissions. Further, the future climate scenarios suggest that the sustainability of low-elevation fens may be in jeopardy, as losses of C exceed inputs.

AKNOWLEDGEMENTS

I owe a lot of gratitude to everyone who helped me on my path to earning this PhD. I'm very thankful that David Cooper gave me the great opportunity to pursue a research career. He served as a great advisor along the way, and I learned a lot working with him. All of my committee members also spent countless hours of their time helping me the past few years and I also owe them a great deal of thanks. Kate Dwire gave me a copy of *The Biology of Peatlands* as soon as I started, and that has been a great reference during the past few years. She also spent several hours in the field and office which contributed to my PhD being a success. Rob Hubbard was extremely helpful in designing soil gas flux chambers and going over my C flux models, as well as providing me with reality checks along the way, in terms of what I could actually get done over a couple of growing seasons. Joe von Fischer provided my first formal graduate-level introduction to ecosystem ecology in his course during my first semester, and was also very generous in letting me run methane samples in his lab. Mike Ronayne was an invaluable resource throughout my PhD program, both in learning hydrological modeling techniques, as well going over my ideas for my own hydrological research.

Tom Hobbs and Phil Chapman each spent several hours with me going over my Bayesian carbon flux models, and were both critical in the model development process. I am also very thankful for all the folks in the Cooper Lab and von Fischer Lab who helped with work in the field and the lab, and provided valuable feedback on my analyses and research ideas throughout the past few years.

Lastly, I wouldn’t be finishing a PhD in Ecology without the help and encouragement of my family. My wife, Chrissy, has been nothing but supportive since we both moved to Fort Collins several years ago. I know conversations about ecological modeling, and parameter estimation must have gotten old on our walks into Old Town, but she was always there to talk about the trials and tribulations associated with getting a PhD. I also owe a great deal of thanks to my parents and brother. Colin helped out with field and lab work along the way, and my parents instilled an appreciation of nature, science, and hard work in me at an early age.

TABLE OF CONTENTS

1 Introduction

Peatlands are wetland ecosystems characterized by the accumulation and persistence of organic soils. Organic matter accumulates because primary production exceeds decomposition due to anaerobic soil conditions. Although peatlands only comprise approximately 3% of the earth's land surface area they store approximately one third of global terrestrial carbon (C) (Gorham, 1991). Because peatlands accumulate organic matter over relatively long periods of time, they have played an important role as stable, long term carbon dioxide (CO_2) sinks. Globally, these ecosystems have had a net cooling effect over the past several millennia despite being one of the largest natural sources of CH_4, a much more potent greenhouse gas (GHG) (Frolking & Roulet, 2007). However, current and future effects of peatland-atmosphere GHG exchange on climate are unclear (Baird *et al*. 2009). Further, predicting future peatland feedbacks to a changing climate requires identifying the important nonlinear and complex ecological and hydrological processes that control GHG in these ecosystems (Belyea 2009).

A water table near the soil surface is a critical control of CO_2 and CH_4 fluxes in peatlands. As water tables decline, near-surface peat is exposed to aerobic conditions and increased ecosystem respiration (ER) can occur (Moore & Knowles, 1989; Chimner & Cooper, 2003), leading to peatlands shifting from CO_2 sinks to sources (Riutta *et al.*, 2007; Wu *et al.*, 2013). Conversely, as water tables rise, they create a reducing soil environment near the biologically active surface peat layers, leading to increased CH_4 efflux to the atmosphere (Moore & Knowles, 1989; Roulet *et al.*, 1992; Turetsky *et al.*, 2007). Therefore, hydrological processes that control water table dynamics in peatlands are of the utmost importance to their ecological functioning, development and persistence, and GHG dynamics (Rydin and Jeglum 2006).

In North America, tens of thousands of relatively small peatlands, dominated by plant species typically found in boreal regions, occur at their southernmost limit in the Rocky Mountains. These peatlands began development following deglaciation, and have accumulated atmospheric C through organic soil development for thousands of years (Chimner *et al.*, 2002). Peatlands found in this region are classified as fens, fed primarily by groundwater and surface water (Cooper & Andrus, 1994). The majority of precipitation in the United States Rocky Mountains at elevations ≥ 2500 m falls as snow (Serreze *et al.*, 1999). Since most, if not all peatlands in this region also occur at elevations ≥ 2500 m (Chimner *et al.*, 2010), direct snow melt and snow melt-derived groundwater and surface water account for the majority of hydrological inputs to these ecosystems. In addition to snow meltwater inputs, portions of the southern Rocky Mountains are also affected by monsoon driven precipitation in late summer (Anderson & Roads, 2002).

Climatic warming and changes in hydrological cycles of mountain regions in the western United States are likely to change as a result of anthropogenic influences (Barnett *et al.*, 2008; Ashfaq *et al.*, 2013; Liu *et al.*, 2013). Increasing air temperatures over recent decades in the Rocky Mountains have reduced peak annual snow water equivalent (SWE) as a result of reduced snowfall and increased winter rainfall, consequently leading to earlier melting of snowpack. This has led to earlier spring stream flows and reduced summer flows (Rood *et al.*, 2008; Clow, 2010), and this trend is expected to continue in the future (Rauscher *et al.*, 2008; Gray & McCabe, 2010; Godsey *et al.*, 2014).

It is unclear how mountain fen C dynamics and hydrological processes vary with elevation and the influence of monsoon precipitation, or how ecosystem processes may change under a future climate regimes. In this dissertation I address the following questions: 1) How

does ecosystem-atmosphere CO_2 exchange vary with elevation and monsoon influence in Rocky Mountain peatlands? 2) How do snowmelt dynamics at high and low elevations and varying monsoon influence affect WT dynamics in fens of the Rocky Mountains? 3) How will mountain fen hydrological dynamics likely change under a future climate, and what will be the likely subsequent impact on ecosystem-atmosphere C exchange?

References

Anderson BT, Roads JO (2002) Regional simulation of summertime precipitation over the southwestern United States. *Journal of Climate*, **15**, 3321–3342.

Ashfaq M, Ghosh S, Kao S-C et al. (2013) Near-term acceleration of hydroclimatic change in the western U.S. *Journal of Geophysical Research: Atmospheres*, **118**, 10,676–10,693.

Baird, AJ, Comas, X, Slater, LD, et al. (2009) Understanding carbon cycling in northern peatlands: recent developments and future prospects. In Carbon cycling in northern peatlands *Geophysical Monograph Series*, **184**, edited by A. J. Baird et al., pp. 1–3, AGU, Washington, D. C.

Barnett TP, Pierce DW, Hidalgo HG et al. (2008) Human-Induced Changes United States. *Science*, **319**, 1080–1083.

Belyea, LR (2009) Nonlinear dynamics of peatlands and potential feedbacks on the climate system, in Carbon Cycling in Northern Peatlands, *Geophysical Monograph Series*, **184**, edited by A. J. Baird et al., pp. 5–18, AGU, Washington, D. C.

Chimner RA, Cooper DJ (2003) Influence of water table levels on CO2 emissions in a Colorado subalpine fen: an in situ microcosm study. *Soil Biology and Biochemistry*, **35**, 345–351.

Chimner RA, Cooper DJ, Parton WJ (2002) Modeling carbon accumulation in Rocky Mountain fens. *Wetlands*, **22**, 100–110.

Chimner RA, Lemly JM, Cooper DJ (2010) Mountain Fen Distribution, Types and Restoration Priorities, San Juan Mountains, Colorado, USA. *Wetlands*, **30**, 763–771.

Clow DW (2010) Changes in the Timing of Snowmelt and Streamflow in Colorado: A Response to Recent Warming. *Journal of Climate*, **23**, 2293–2306.

Cooper DJ, Andrus RE (1994) Patterns of vegetation and water chemistry in peatlands of the west-central Wind River Range, Wyoming, U.S.A. *Canadian Journal of Botany*, **72**, 1586–1597.

Frolking S, Roulet NT (2007) Holocene radiative forcing impact of northern peatland carbon accumulation and methane emissions. *Global Change Biology*, **13**, 1079–1088.

Godsey SE, Kirchner JW, Tague CL (2014) Effects of changes in winter snowpacks on summer low flows: case studies in the Sierra Nevada, California, USA. *Hydrological Processes*, **28**, 5048–5064.

Gorham E (1991) Northern peatlands: Role in the carbon cycle and and probable response to climatic warming. *Ecological Applications*, **1**, 182–195.

Gray ST, McCabe GJ (2010) A combined water balance and tree ring approach to understanding the potential hydrologic effects of climate change in the central Rocky Mountain region. *Water Resources Research*, **46**, W05513.

Liu Y, L. Goodrick S, A. Stanturf J (2013) Future U.S. wildfire potential trends projected using a dynamically downscaled climate change scenario. *Forest Ecology and Management*, **294**, 120–135.

Moore TR, Knowles R (1989) The influence of water table levels on methane and carbon dioxide emmisions from peatland soils. *Canadian Journal of Soil Science*, **69**, 33–38.

Rauscher S a., Pal JS, Diffenbaugh NS, Benedetti MM (2008) Future changes in snowmelt-driven runoff timing over the western US. *Geophysical Research Letters*, **35**, 1–5.

Riutta T, Laine J, Tuittila E-S (2007) Sensitivity of CO_2 Exchange of Fen Ecosystem Components to Water Level Variation. *Ecosystems*, **10**, 718–733.

Rood SB, Pan J, Gill KM, Franks CG, Samuelson GM, Shepherd A (2008) Declining summer flows of Rocky Mountain rivers: Changing seasonal hydrology and probable impacts on floodplain forests. *Journal of Hydrology*, **349**, 397–410.

Roulet NT, Moore TR, Bubier JL, Lafleur PM (1992) Northern fens: methane and climate change. *Tellus B*, **44**, 100–105.

Rydin, H and Jeglum, J (2006) *The Biology of Peatlands*. Oxford University Press. p. 138.

Serreze MC, Clark MP, Armstrong RL, McGinnis DA, Pulwarty RS (1999) Characteristics of the western United States snowpack from snowpack telemetry(SNOTEL) data. *Water Resources Research*, **35**, 2145–2160.

Turetsky MR, Wieder RK, Vitt DH, Evans RJ, Scott KD (2007) The disappearance of relict permafrost in boreal north America: Effects on peatland carbon storage and fluxes. *Global Change Biology*, **13**, 1922–1934.

Wu J, Roulet NT, Sagerfors J, Nilsson MB (2013) Simulation of six years of carbon fluxes for a sedge-dominated oligotrophic minerogenic peatland in Northern Sweden using the McGill Wetland Model (MWM). *Journal of Geophysical Research: Biogeosciences*, **118**, 795–807.

2 Mountain peatlands range from CO_2 sinks at high elevations to sources at low elevation: Implications for a changing climate

2.1 Introduction

Mountains cover approximately one quarter of the earth's surface and create strong climate gradients, as temperature and precipitation regimes vary significantly with elevation and landscape position over relatively short distances (Cooper *et al.* 2012). As a result, mountains typically support high biodiversity, with a range of ecosystems and species assemblages along elevation and aspect gradients (Beniston, 2003). Sometimes referred to as "sky islands", mountain ecosystems may be geographically isolated, surrounded by distinctly different climate conditions at lower elevations that cannot support their existence (Warshall, 1994). These ecosystems and their biota are particularly susceptible to the effects of a warming climate, and an upward shift in the elevation range of several species and habitats has been observed in mountains throughout the world (Parmesan, 2006). Examples include rising tree lines, and the movement of pikas to higher elevations in western North America as the lower boundaries of their historic ranges become less suitable (Krajick, 2004). While climate often controls the lower elevation limit of mountain species and ecosystems, the upper elevation limit can be determined by topography, as is the case with mountain peatlands (Cooper *et al.* 2012).

Peatlands are among the most valuable ecosystems in mountains, providing critical perennially wet habitat for wildlife, supporting high biodiversity, and sustaining rare plant species that are in some cases isolated from their nearest population by over 1000 km (Cooper, 1996; Chimner *et al.*, 2010). Further, these ecosystems have sequestered atmospheric carbon dioxide (CO_2) for several millennia, serving as regionally significant carbon (C) sinks (Chimner *et al.*, 2002). Groundwater-fed peatlands (fens) dominated by wetland plant species whose main

distribution is in boreal regions, exist at their southernmost limit in mountain regions of western North America (Cooper and Andrus 1994, Chimner *et al.* 2010, Cooper *et al.* 2012). In these regions, temperature decreases, and in most areas, precipitation increases with elevation. Snowmelt-derived water provides the hydrologic support for fens in western North America that rarely occur below elevations with a large winter snow pack (Chimner *et al.* 2010). Late-summer precipitation driven by the North American Monsoon is also an important seasonal water source in the southwestern US. However, monsoon precipitation is most consistent in mountain regions located closest to the desert southwestern US.

A changing climate has led to earlier spring snow melt and runoff, and a reduction in total mountain snowpack in the western US, with more winter precipitation falling as rain instead of snow (Regonda *et al.*, 2004; Christensen & Lettenmaier, 2007; Ashfaq *et al.*, 2013). This shift in the timing of key hydrological processes has reduced late-summer stream flows and created deeper water table drawdowns, increasing drought stress in riparian ecosystems (Rood *et al.*, 2008). In the Rocky Mountains, regionally variable monsoon influences further complicates efforts to predict how growing season hydrological cycles could be affected by climate change. It is uncertain whether local and regional hydrological processes can sustain mountain fens, but it is likely that warming air temperatures and subsequent changes in watershed hydrological dynamics will impact C cycling in these ecosystems.

One of the defining ecological characteristics of peatlands is C sequestration, resulting in the formation of organic soils. This process has led peatlands to store approximately one third of global terrestrial C (Gorham, 1991). Carbon dioxide dynamics are the primary control on peatland C balance, and play a key role in their development and persistence. Net ecosystem production (NEP) represents the difference between gross primary production (GPP) and

ecosystem respiration (ER) and when positive, represents a gain of CO_2 to an ecosystem, and a loss to the atmosphere when negative (Chapin *et al.*, 2006). Water tables near the soil surface during the growing season are a key driver of C accumulation, as it maintains low rates of ER relative to GPP. As water tables drop, more of the soil profile is exposed to aerobic conditions that can increase ER, leading to a reduction in NEP, particularly for fens (Chimner & Cooper, 2003a; Riutta *et al.*, 2007; Wu *et al.*, 2013). Further, warmer air temperatures increase can decrease NEP by increasing ER, particularly when water tables are lower than the peat surface (Sullivan *et al.*, 2007).

Changes in hydrological regime cause significant lowering of the water table in mountain fens during the growing season coupled with increased air temperature could reduce annual NEP in mountain fens, which would have critical implications for the long-term sustainability of these ecosystems. We hypothesized that this process would be most significant for fens at the low end of their known elevation range since they already experience warmer climate conditions and have low snowpack. In this study, we developed empirical models of CO_2 dynamics driven by meteorological and hydrological variables and estimated CO_2 fluxes over two growing seasons for four mountain fens. The fens were located near the low and high ends of their known elevation range in two regions that receive different amounts of monsoon precipitation. Our objectives were to i) identify trends between growing season NEP and growing season climate and hydrological conditions, and ii) compare NEP among mountain fen plant communities occurring at the high and low ends of their elevation range, and in regions with different monsoon influence.

2.2 Study Sites

We studied four rich fens, two in the Medicine Bow Mountains of southern Wyoming, and two in the San Juan Mountains of southwestern Colorado (Table 2.1). In each study region we chose one fen located near the lower end and one near the upper end of the known elevation range for this ecosystem type (Chimner *et al.*, 2010). Mean annual and growing season air temperature among sites decreases with increasing elevation and latitude. Average snowfall increases with elevation in the study sites, and average precipitation during the summer varies between the two study regions. The North American Monsoon has a stronger influence in the San Juan Mountains where the wettest months of the year occur in late summer. Data was collected from two SNOTEL telemetric micrometeorological stations, the Cascade station (ID: 386, elevation: 2710 m) in the San Juan Mountains and the Brooklyn Lake station (ID: 367, elevation: 3120 m)in the Medicine Bow Mountains, to provide a long-term (1983-2013) perspective on SWE, growing season precipitation, and air temperature in each study region.

Anglica Fen (ANG) was the low elevation San Juan Mountains study site, located in a basin surrounded by granite bedrock outcrops with no surface water inflows or outflows. At this site, we studied one community dominated by *Carex lasiocarpa* (ANG-LAS) and another by *C. lasiocarpa* and *C. utriculata* (ANG-LUT). Spruce Fen (SPR), the high elevation site in the San Juan Mountains, occurs on a gentle slope with a surface water inflow and outflow. The two plant communities studied at SPR were dominated by *C. utriculata* (SPR-UTR), and *C. saxatilis* (SPR-SAX). Sand Lake Fen (SLK), the low elevation Medicine Bow Mountains study site, is surrounded by glacial moraine deposits with no surface water inflow and an ephemeral surface water outlet. The two plant communities studied occurred as a mosaic and were dominated by *Salix planifolia*, *S. wolfii* and *Betula glandulosa* (SLK-BET) and another dominated by *C. simulata, C. utriculata* and *Juncus balticus* (SLK-SIM). Medicine Bow Peak Fen (MBP), the

high elevation site in the Medicine Bow Mountains, occurs on a gentle slope and receives a portion of its water input from a point of groundwater discharge. At MBP we studied a community dominated by *S. planifolia* and *S. wolfii* (MBP-PLA), and another dominated by *C. aquatilis* (MBP-AQU).

2.3 Methods

Precipitation

During the winter months, Moultrie Game Spy cameras were installed at each site and programmed to photograph the majority of the fen, including a centrally located snow depth gauge marked at 5-cm increments, to track daily changes in snow depth and determine when each site became snow-free. Peak snow water equivalent (SWE) at each site was determined using snow depth data collected by the on-site cameras. A 2^{nd} order polynomial function, fit to data collected at nearby SNOTEL stations, was used to model SWE as a function of on-site snow depth (See Chapter 2 for further details). Growing season rain events for each study region were recorded at the low elevation sites using Hobo Onset RG-2 data logging rain gauges (Bourne, MA).

CO_2 flux measurements

Fluxes of CO_2 were measured in three plots in each plant community in each fen. ABS plastic collars, 60 cm x 60 cm, inserted approximately 5 cm into the soil, were used as the base for a 2.16 $x10^5$ cm^3 cubic gas flux chamber. The chamber consisted of an aluminum frame and clear acrylic panels that allowed >90% of PAR to pass through. A channel containing closed-cell foam along the bottom of the chamber ensured an air-tight seal between the chamber and collars. Because it was not possible to install collars and make chamber-based gas flux measurements in

areas dominated by *S. planifolia* due to the height and density of the shrubs, for SLK-BET, *B. glandulosa* was chosen for gas flux plots to represent the shrub stands. Measurements were made in the field using a PP-Systems EGM-4 infrared CO_2 gas analyzer (IRGA) (Amesbury, Massachusetts). Concentrations of CO_2 were measured at 5-sec intervals over a 2-min period and the quadratic slope of the change in concentration over time was used to calculate the flux (Johnson *et al.*, 2013). Two battery powered fans within the chamber mixed the air during measurement periods, and on hot mid-summer days, ice packs were mounted in the chamber to prevent overheating of chamber air.

Measurements of CO_2 fluxes were made on an approximately biweekly basis during the growing season of 2011, monthly during 2012, and once in August 2013 at SLK and ANG, when the water table was at its lowest position during the study for SLK. During 2011, mid-day NEP was measured using the clear chamber followed by measurements of ER using a light-proof cover over the chamber. Gross primary production was determined by summing concurrent NEP and ER flux rates (both positive in this case). During the 2012 growing season and in August 2013, fluxes were measured several times during each field day. Measurements using the clear chamber were followed by measures with two shade clothes covering the chamber, reducing PAR by 75% and 50%, followed by an ER measurement using a light proof cover. This approach allowed for a greater range of PAR used in fitting models to measured fluxes. During each measurement, PAR and air temperature within the chamber were recorded, as well as water table position in monitoring wells adjacent to each collar.

Modeling carbon dioxide fluxes

We modified equations used by Riutta and others (2007) to model GPP and ER. GPP was modeled for each plant community as a function of PAR and a seasonality term based on a four-week running average (21 days before, 7 days after) of daily mean air temperature (RAV) [Equation 1]. A rectangular hyperbola function was used to model ecosystem photosynthetic response to incoming PAR, and a Gaussian function was used for the seasonality term, allowing modeled GPP to follow seasonal dynamics associated with plant phenology.

$$\boldsymbol{GPP_i = \frac{A_{max} * \alpha * PAR_i}{A_{max} + \alpha * PAR_i} * e^{\left[-0.5\left(\frac{RAV_i - RAV_{optGPP}}{RAV_{devGPP}}\right)^2\right]}} \quad \textbf{(1)}$$

In Equation 1, A_{max} (g CO_2-C m^{-2} hr^{-1}) represents the asymptotic maximum potential rate of GPP, and α (g CO_2-C µmol PAR^{-1}) represents the light use efficiency, or initial slope of the light response function. The parameter RAV_{optGPP} (C°) represents the optimum value of RAV for GPP and RAV_{devGPP} (C°) represents the standard deviation of the Gaussian function, which controls the spread of the distribution.

Ecosystem respiration was modeled as a function of air temperature (AT), water table position (WTP), and a seasonality term [Equation 2]. A modified van't Hoff equation was used to model ER as increasing exponentially with air temperature. The response of ER to water table position was modeled as a negative exponential equation, and a Gaussian function similar to that of the GPP model was used to account for seasonal variation in ER.

$$\boldsymbol{ER_i = R_{10} * Q_{10}^{\left(\frac{AT_i - 10}{10}\right)} * e^{-b * WTP_i} * e^{\left[-0.5\left(\frac{RAV_i - RAV_{optER}}{RAV_{devER}}\right)^2\right]}} \quad \textbf{(2)}$$

In Equation 2, R_{10} (g CO_2-C m^{-2} hr^{-1}) represents ER at 10°C when other model factors are not limiting, Q_{10} represents the rate of increase in ER per 10°C increase in air temperature, b (g m^{-2} cm^{-1}) represents the initial slope of the rate of increase in ER per decrease in water table position below the peat surface. RAV_{optER} (C°) and RAV_{devER} (C°) represent the optimum RAV value for ER and the standard deviation of the Gaussian function controlling seasonality in ER, respectively.

Model development and evaluation

We fit models to the measured data using Bayesian methods in R statistical software. Model parameters were estimated using Markov chain Monte Carlo (MCMC) analysis in the *rjags* package for R (Plummer, 2011). A total of 100,000 iterations were used with 4 MCMC chains, with burn-in after 30,000 iterations. Vague priors were used for all model parameters. Uniform distributions with limits ranging between 0 and 30 were used for RAV_{optGPP}, RAV_{devGPP}, RAV_{optER}, and RAV_{devER} priors, uniform distributions with limits ranging between 0 and 0.1 were used for α priors, gamma distributions with shape and rate parameters equal to 0.001 were used for A_{max}, $\sigma_{procGPP}$, R_{10}, Q_{10}, and σ_{procER} priors, and a beta distribution with both shape parameters equal to 1 was used for the b priors. We used mean-weighted variance in modeling GPP and ER in order to account for variance that increased with both flux rates (Equations 3 and 4).

$$\boldsymbol{GPP_i^{obs} \sim Normal(\mu GPP_i, \sigma_{procGPP} * \mu GPP_i)} \quad \textbf{(3)}$$

$$\boldsymbol{ER_i^{obs} \sim Normal(\mu ER_i, \sigma_{procER} * \mu ER_i)} \quad \textbf{(4)}$$

Equations 3 and 4 represent the likelihood functions for the observed GPP (GPP_i^{obs}) and ER (ER_i^{obs}) measured in each plant community. In the equations, μGPP_i and μER_i represent the predicted values of GPP and ER, respectively, and $\sigma_{procGPP}$ and σ_{procER} represent the process variance associated with those predictions.

Modeling growing season CO_2 fluxes

Once model parameters were estimated, GPP and ER models were run for all sites, for the period May 28 through September 19 in 2012 and 2013. Models were run using hourly PAR, air temperature, and water table position measured throughout both growing seasons. Continuous PAR measurements were recorded using a Campbell Scientific CR10X data logger (Logan, UT) equipped with an Apogee Instruments SQ-110 quantum sensor (Logan, UT). PAR measurements used to drive growing season GPP models for the San Juan sites and Medicine Bow sites were made at the respective low elevation sites in each of these regions. At each site, an In-Situ Barotroll logger (Fort Collins, CO) was used to record hourly air temperature. In-Situ Rugged Troll pressure transducers were used to measure hourly water table position in monitoring wells installed in each plant community. Because of the patchy distribution of shrub and graminoid communities at SLK, and no obvious hummock-hollow microtopography, one pressure transducer was used for both communities. During the study, the water table fell below the elevation of the monitoring well pressure transducer at ANG-LUT and SPR-UTR. This resulted in several periods without data, and models were run with the water table at -54 cm from 7/20/12 to 7/31/12, 8/20/12 to 9/18/12, 6/28/13 to 6/29/13, and 7/12/13 to 9/18/13 for ANG-LUT, and -16 cm from 6/24/13 to 7/3/13, 8/11/13 to 8/22/13, 9/4/13 to 9/11/13, and 9/15/13 to 9/18/13 for SPR-UTR.

Hourly and growing season GPP and ER were estimated using MCMC, with a total of 6,000 iterations and burn-in at 3,000 iterations. Hourly and growing season NEP estimates were determined similarly, as the difference between GPP and ER.

Once growing season CO_2 flux estimates were determined, we developed a Bayesian Multiple Linear Regression (BMLR) model using mean growing season air temperature and water table position as predictor variables and mean growing season NEP as the response variable (Equation 5).

$$\boldsymbol{NEP_j = \beta_0 + \beta_1 AT_j + \beta_2 WTP_j} \quad \textbf{(5)}$$

NEP is the mean growing season NEP, determined using the hourly time step deterministic models, *AT* is mean growing season air temperature (°C), and *WTP* is mean growing season water table position (cm). β_0, β_1, and β_2 represent regression coefficients, all of which had normal distributions for vague priors with shape parameters of 0 and 1 x 10^{-6} for mean and variance, respectively. Equation 6 represent the likelihood function for growing season NEP ($NEP_j^{modeled}$) for each plant community, derived using the previously described deterministic models.

$$\boldsymbol{NEP_j^{modeled} \sim Normal(\mu NEP_j, \sigma_{procNEP})} \quad \textbf{(6)}$$

In Equation 6, μNEP_j represents the predicted values of growing season NEP using the BMLR model, and $\sigma_{procNEP}$ represents the process variance associated with those predictions. Parameters for the BMLR models were also estimated using MCMC, with a total of 25,000 iterations, and burn-in at 10,000 iterations.

I used the Gelman-Rubin diagnostic to ensure model convergence for all parameters and model predictions (Gelman & Rubin, 1992).

2.4 Results

Growing season climate and hydrological conditions

Mean growing season air temperature decreased with increasing elevation across sites during both study years (Table 2.2). The warmest mean growing season air temperature, 15.4°C, occurred at ANG in 2012, while the coldest occurred at the highest site, SPR, 10.5 °C in 2012 and 2013. With the exception of MBP in 2012, the high elevation sites had greater peak SWE than the low elevation sites in each region. During both study years the San Juan Mountains sites had higher peak SWE than their counterparts in the Medicine Bow Mountains. Within each region, the low elevation sites were snow-free from several days to approximately a month earlier than the high elevation sites (Table 2.2). In 2012, both Medicine Bow sites were snow-free by April 2, more than a month earlier than in 2013, and earlier than both San Juan sites in 2012.

The San Juan Mountains received 77-94% more summer precipitation than the Medicine Bow Mountains. June precipitation ranged from 5-16 mm for both regions. However, late-summer precipitation (July-August) in the San Juan Mountains was 40-71 mm in 2012 and 2013, compared with 17-40 mm for the Medicine Bow Mountains. The 2013 growing season was wetter than 2012 in both regions, in part due to unusually high precipitation during September (Table 2.2, Figure 2.1).

The two high elevation fen water tables averaged 19 cm closer to the soil surface than the low elevation sites (Table 2.2). Within both regions, low elevation sites had the earliest water table decline (Figure 2.1).

Peak SWE in 2012 and 2013 was below the 20-yr average in both regions. In particular, 2012 had the 3rd lowest peak SWE since 1983 in the Medicine Bow Mountains. June through August precipitation was below average in both study regions during the study years, however deviation from the mean was most significant in the Medicine Bow Mountains where rainfall was approximately half of the 20-yr average. Both SNOTEL sites had an increase in mean annual air temperature of approximately 0.2°C yr^{-1}, from 1990 to 2013 ($0.62 \leq R^2 \leq 0.67$). Thus, mean growing season air temperatures among all sites were higher than average for the prior two decades.

Gross primary production and ecosystem respiration – growing season fluxes and model parameter estimates

Field-measured GPP rates ranged from 0.003 to 1.26 g CO_2-C m^{-2} hr^{-1} across measurement years, and increased with elevation within each region and with latitude between the high and low sites in each region (Figure 2.2). Similarly, mean growing season GPP generally increased with elevation and latitude (Figure 2.3). During both study years, mean growing season GPP was lowest for ANG-LAS, 373 g CO_2-C m^{-2} in 2012 and 350 g CO_2-C m^{-2} in 2013. Highest growing season GPP estimates during both study years were observed in MBP-PLA, ranging from 780 g CO_2-C m^{-2} in 2012 and 741 g CO_2-C m^{-2} in 2013.

Field-measured ER rates ranged from 0 to 0.53g CO_2-C m^{-2} hr^{-1} across measurement years, and followed a similar trend as measured GPP, increasing with elevation within regions and with latitude between high and low sites between regions (Figure 2.2). However, unlike growing season estimates of GPP, mean growing season ER was more variable among and within sites (Figure 2.3). The lowest mean growing season ER occurred in the two SPR

communities during both years with rates ranging from 304 to 348 g CO_2-C m^{-2} for both plant communities. Highest mean growing season ER occurred in both years at the Medicine Bow sites. In 2012, the highest ER occurred at MBP, with 596 g CO_2-C m^{-2} for MBP-AQU and 542 g CO_2-C m^{-2} for MBP-PLA. In 2013, the highest mean growing season ER occurred at SLK, with rates of 960 g CO_2-C m^{-2} for SLK-SIM and 629 g CO_2-C m^{-2} for SLK-BET.

Variability of net ecosystem production among sites

Net ecosystem production in each fen was similar between years for the San Juan sites. In the Medicine Bow Mountains, SLK had much lower NEP in 2013 than 2012, driven by a lower water table in 2013. Conversely, NEP at MBP-PLA was similar between years, while MBP-AQU increased approximately two-fold between 2012 and 2013, which corresponded to an increase in mean growing season water table position between years (Table 2.2, Figure 2.3).

The lowest rates of growing season NEP in 2012 occurred at ANG, with ANG-LAS representing the only negative NEP estimate, -25 g CO_2-C m-2, for this during this study year. ANG-LUT represented the lowest positive rate of NEP at 18 g CO_2-C m^{-2}. In 2013, the lowest rates of NEP occurred at the two SLK plant communities, -342 g CO_2-C m^{-2} for SLK-SIM and -53 g CO_2-C m^{-2} for SLK-BET. In addition, NEP was lower for both plant communities at ANG in 2013, with rates of -43 g CO_2-C m^{-2} for ANG-LAS and 32 g CO_2-C m^{-2} for ANG-LUT. The highest rates of growing season NEP occurred at the high elevation sites in both years of the study, 237 g CO_2-C m^{-2} for MBP-PLA in 2012, and 256 g CO_2-C m^{-2} for SPR-UTR in 2013 (Table 2.2, Figure 2.3).

The BMLR model revealed that mean growing season NEP decreased with increasing mean growing season air temperature, and with decreasing mean growing season water table position

(R^2 = 0.67) (Table 2.3). Among plant communities, and sites, NEP generally increased with elevation (Figure 2.3, Figure 2.4). This was particularly true for the San Juan fens where, on average, NEP was an order of magnitude higher at SPR than ANG in both years. NEP was an order of magnitude higher at MBP than SLK in the Medicine Bow in 2013, while in 2012, NEP was slightly higher at SLK than MBP.

2.5 Discussion

Climate and hydrological controls on net ecosystem production

Growing season NEP was negatively correlated with mean growing season air temperature and positively correlated with mean growing season water table position (Figure 2.4). Further, NEP decreased with temperature increases of a few degrees Celsius, ranging from positive to negative. This is in concordance with recent findings from a subarctic fen in northern Sweden (Wu *et al.*, 2013). Likewise, the decrease in NEP with declining water table position observed in this study mirrors that of peatlands in boreal regions of Europe and North America (Bubier *et al.*, 2003; Riutta *et al.*, 2007), and in the Rocky Mountains (Chimner & Cooper, 2003a; Schimelpfenig *et al.*, 2013).

These trends caused NEP to increase with elevation. The high elevation fens functioned as CO_2 sinks, with a mean NEP rate of 195 g CO_2-C m^{-2} for the four plant communities analyzed. The rates for SPR and MBP are similar to those reported in higher latitude peatlands with similar vegetation (Riutta *et al.*, 2007; Adkinson *et al.*, 2011; Maanavilja *et al.*, 2011). The low elevation fens had much lower growing season NEP, with net losses of CO_2 for one or both of the study years, and an overall mean NEP rate of about 1 g CO_2-C m^{-2}, which were similar to CO_2 fluxes reported for hydrologically modified fens in the Rocky Mountains (Chimner & Cooper, 2003b).

It is important to consider that the growing season represents a relatively small fraction of the year in montane and subalpine environments. Wintertime fluxes of CO_2 have been identified as being an important contribution to overall annual CO_2 balance of boreal peatland ecosystems (Aurela, 2002). Mast *et al.* 1998 reported an average wintertime NEP rate of -7.2×10^{-3} g CO_2-C m^{-2} hr^{-1} for a subalpine fen dominated by *C. aquatilis* and *C. utriculata*, located in the Rocky Mountains of Colorado. Applying this average flux rate to the remaining 250 days of the year outside the growing season study period, results in a total NEP flux of 49 g CO_2-C m^{-2} $winter^{-1}$. NEP on an annual basis is therefore much lower than NEP when considering only the growing season. Such reductions have critical implications for low elevation fens, considering there were several instances of negative growing season NEP at the low elevation fens in this study. In particular, annual NEP for both ANG plant communities would be negative, acting as a CO_2 source during both years of this study.

Elevation and monsoon effects on fen net ecosystem production

This study was able to capture trends in peak SWE and timing of snow melt associated with elevation that are typical of mountain regions in the western US (Moore *et al.*, 2014). The low elevation fens had lower peak SWE and earlier snowmelt due to warmer early summer air temperatures, resulting in a longer snow-free season than the higher elevation sites. Earlier snow melt led to an earlier decline in water tables during the growing season at both low elevation fens, even though they exist in different hydrogeological settings. This contributed to higher ER relative to GPP, and lower NEP compared to the high elevation sites that maintained shallow water tables throughout most of the growing season.

We estimated growing season CO_2 fluxes from 5/28 to 9/19 during both study years at all sites, regardless of when they became snow-free. This allowed for comparisons of CO_2 fluxes to be made among sites during the same time period in both years, but did not account for the time period between melt out and the start of our model simulations, which was highest at the low elevation sites, over a month in some cases. However, NEP between the timing of snow melt and the start of the model simulations was likely quite low, possibly negative, due to relatively low plant biomass in the spring (Blanken, 2014), as well as lower daily PAR inputs and higher rates of nighttime ER associated with shorter day length earlier in the year (Wohlfahrt *et al.*, 2013).

Although the San Juan sites received almost double the growing season rainfall as the Medicine Bow sites, there were no discernible differences in fen NEP between these two regions that were directly associated with summer precipitation. While mean growing season water table position was an important predictor of NEP among sites in this study, the response of water tables to precipitation events can be spatially and temporally variable in wetland ecosystems, due to complex factors such as local topography and geomorphology (Tufford, 2011; Vidon, 2012). Growing season NEP estimates at SPR were strongly positive due in part to relatively high water tables. Water tables at SPR varied little during the study years and did not respond strongly to precipitation events. At ANG, which received the same amount of growing season precipitation as SPR, growing season NEP estimates were much lower, due in part to higher ER resulting from lower water tables. Unlike SPR, the water table rose rapidly followed precipitation events at ANG, where rain followed dry periods during which the water table steadily declined. Despite receiving considerably less rainfall from July through August, water tables responded similarly in the Medicine Bow sites, with a rapid rise following rain events at SLK, and more subtle water table rises at MBP.

The disparity in the responses of water tables to precipitation between the high and low elevation sites is likely due to the position of the water table relative to the peat surface, prior to rain events. Saturated hydraulic conductivity (K_s) decreases with depth in peat soils, with surface peat layers being highly conductive, relative to the highly decomposed older peat layers lower in the soil profile (Letts *et al.*, 2000; Schimelpfenig *et al.*, 2013). Therefore, in sloping fens with shallow water tables, like SPR and MBP, it is possible for infiltrated precipitation to move laterally through surface peat layers relatively quickly, dampening the magnitude of water table rise. Further, soil porosity decreases with depth in peat (Letts *et al.*, 2000; Schimelpfenig *et al.*, 2013), increasing the magnitude of water table rise to infiltrated precipitation at lower depths. Although this was the case, since water table decline occurred earlier in the low elevation sites and water tables were considerably lower than that of the high elevation sites during the monsoon season, rises water table were short-lived, and not sufficient at maintaining shallow water tables, comparable to the high elevation sites.

Rocky Mountain fens in a future climate

The strong climate gradient between low and high elevation fens in this study controlled differences in their growing season NEP. Over the coming decades, average annual temperatures are expected to increase by 1.0 to 2.4 °C in the southern Rocky Mountains (Christensen *et al.*, 2004) and reductions in snowpack of 10 - 40% have been predicted for elevations between 2500 and 3000 m in Colorado (Christensen & Lettenmaier, 2007), an elevation range that includes the lower elevation limit for fens in the region (Chimner *et al.* 2010). The changing climate is therefore likely to alter the hydrological regime of mountain fens during the growing season, lowering water tables and consequently decreasing NEP, particularly for low elevation fens.

We observed the lowest rates of growing season NEP in fens at the low end of their known elevation range in both mountain regions. Reductions in NEP associated with a warming climate may convert low elevation fens, with already low positive NEP, from net sinks to net sources of CO_2. Therefore, the long-term sustainability of fens at low to middle elevations in the Rocky Mountains, and other mountain ranges in the western U.S. may be in jeopardy, where their organic soil could be lost through decreased NEP. Furthermore, mountain fens containing sedge-derived peat, like the fens in this study, may be particularly susceptible to increased decomposition resulting from lowered water tables, since most of the CO_2 fixed through GPP is allocated belowground (Chimner *et al.*, 2002).

An important consideration in understanding the long term sustainability of mountain fens to climate change is their hydrogeological and topographic setting. Mountain fens are typically smaller than boreal and subarctic peatlands due to strong topographic confinement in valleys and basins, and relatively small hydrological contributing areas (Patterson & Cooper, 2007). Fens at low elevation may be partially buffered from the adverse effects of climate change, depending on the size and geological nature of the watershed that supports their hydrological regime. For example, fens with watersheds large enough to provide adequate groundwater flows to maintain shallow water tables during the growing season may not experience declines in NEP. It is important to note, however, that ecosystems within mountain fen watersheds, regardless of their size, may experience increased water demands and drought stress due to climate change (Rood *et al.*, 2008) and human uses, such as ground water withdrawals (Cooper *et al.*, 2015). In this case, the potential benefits of a large watershed may be diminished.

The low rates of NEP at the low elevation sites were associated with warmer air temperatures and lesser snowpacks, earlier melt-out, and lower growing season water tables than the high elevation sites. Coupled with predictions of reduced peak SWE and earlier snow melt associated with a warming climate, the results of this study suggest that the elevation ranges that provide climate conditions supportive of mountain fens in the Rocky Mountains are narrowing, with their lower limits shifting upward in elevation. In cases where long-term groundwater and surface water base flows are unable to maintain shallow water tables in mountain fens, over time they may lose the organic soils that define them, through increased decomposition relative to production.

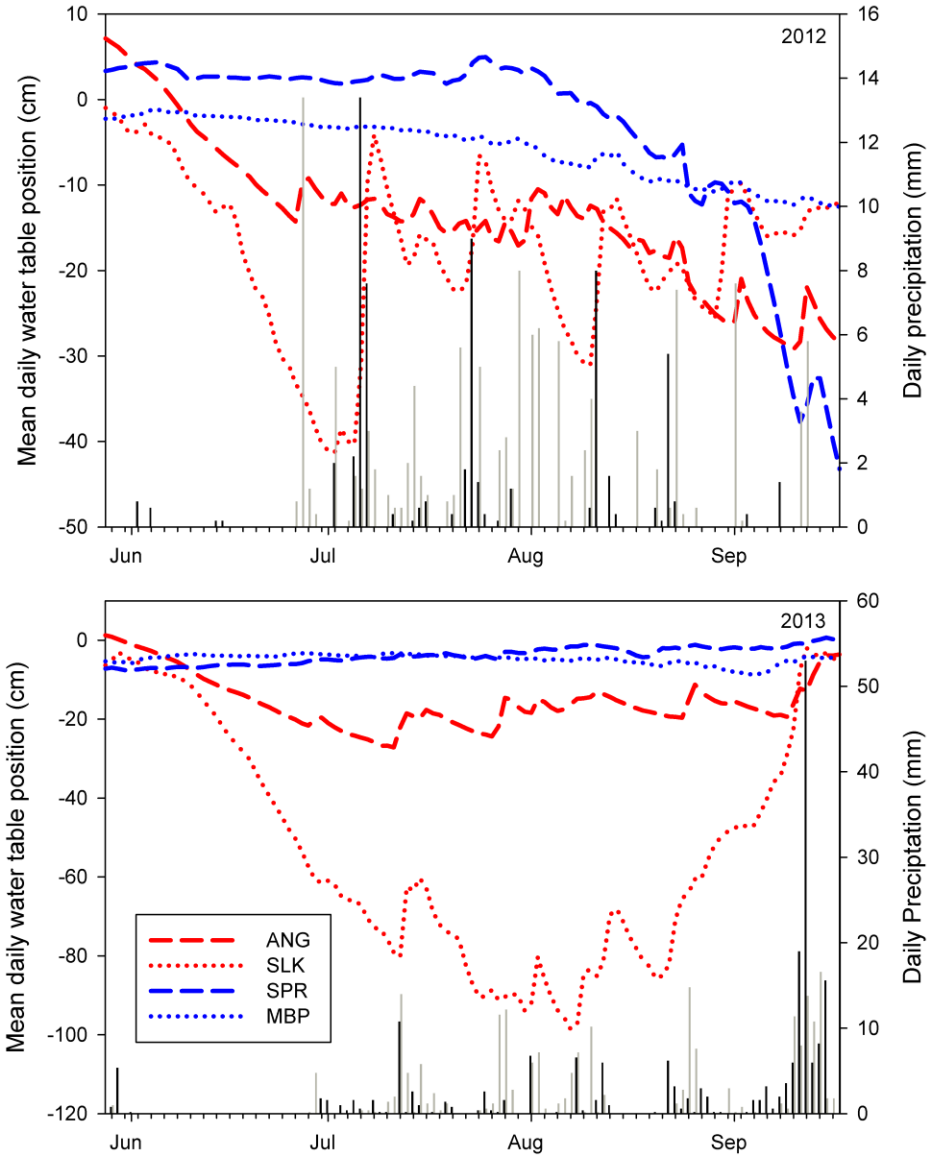

Figure 2.1. Growing season water table dynamics from centrally located monitoring wells for high (blue) and low (red) elevation sites in the San Juan (dashed) and Medicine Bow (dotted) Mountains. Daily precipitation events for the San Juan (grey) and Medicine Bow (black) Mountains are represented as vertical bars.

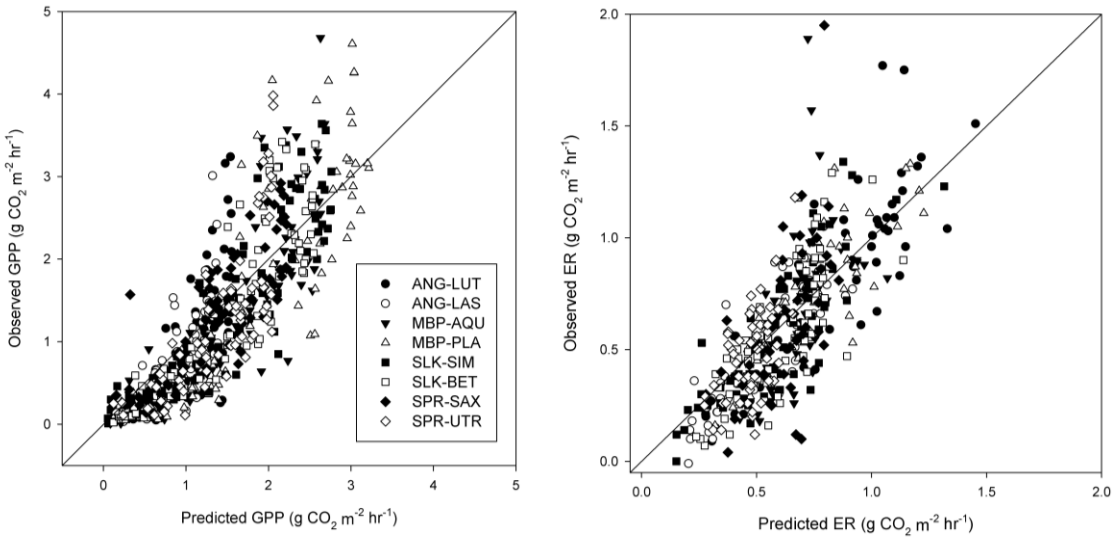

Figure 2.2. Observed versus predicted GPP and ER for all study sites.

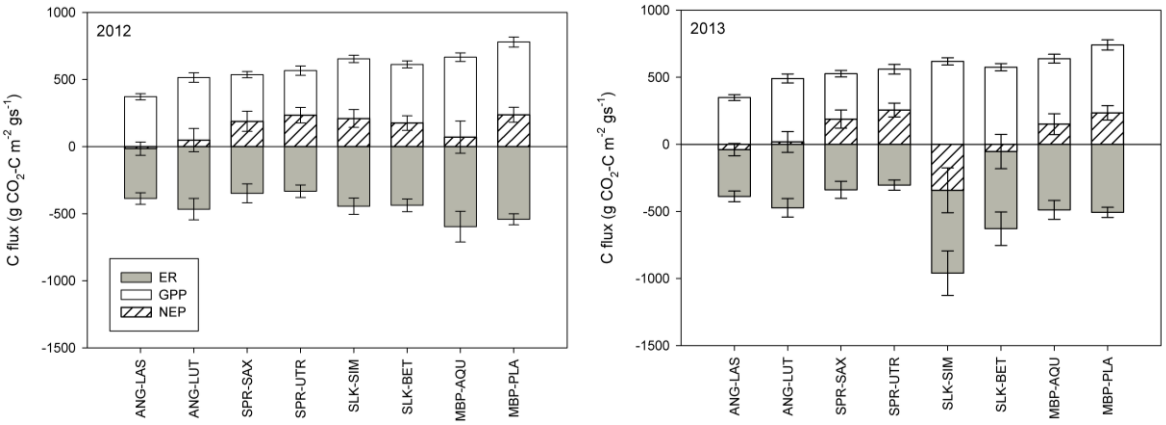

Figure 2.3. Mean growing season estimates of GPP, ER, and NEP among sites during each study year. Error bars represent standard deviation of the posterior mean.

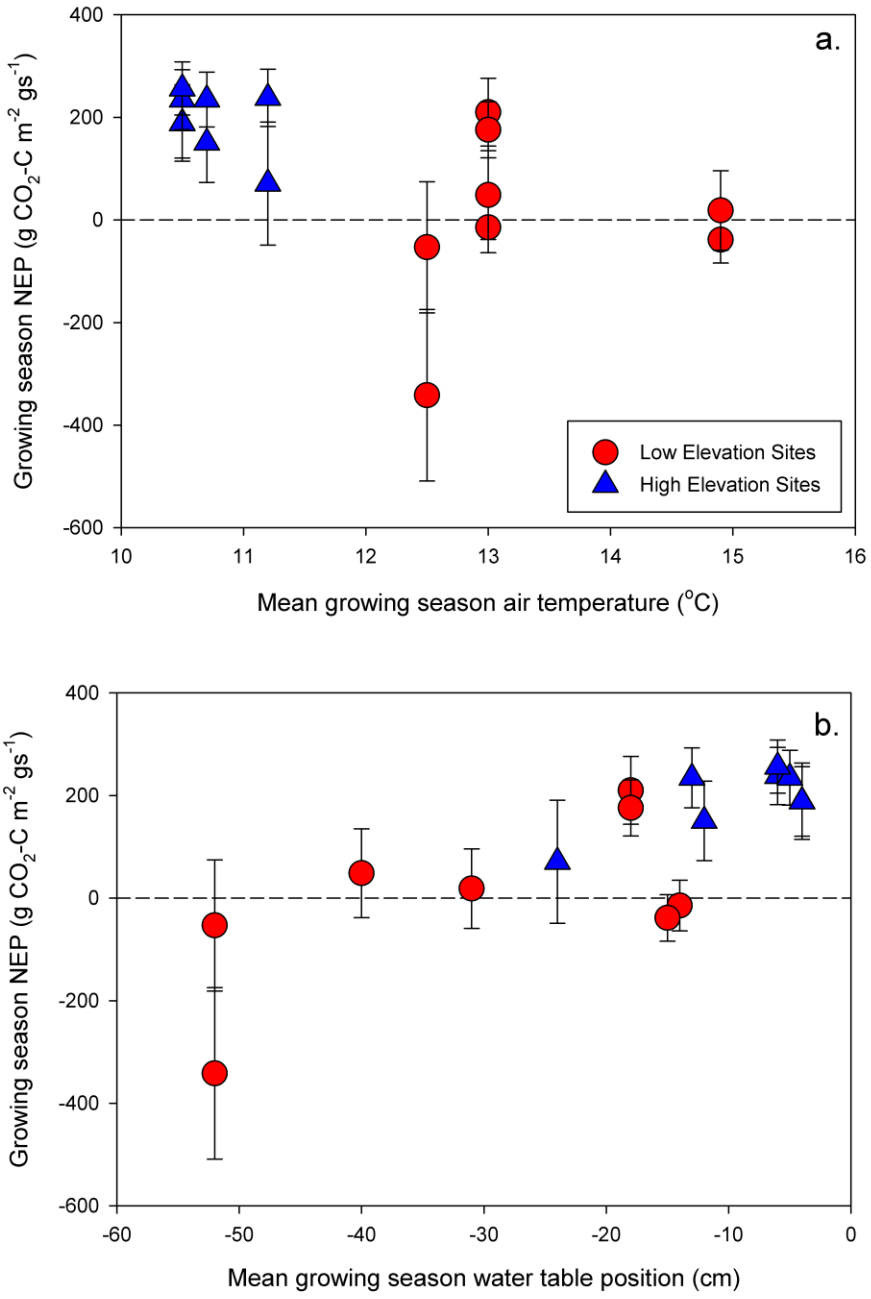

Figure 2.4. Mean growing season NEP versus mean growing season air temperature (a) and mean growing season NEP versus mean growing season water table position (b). Error bars represent standard deviation of the posterior estimate for NEP.

Table 2.1. Study Site Location and Peat Chemical Characteristics.

	Peat chemical properties*								
	Mg (ppm)	Ca (ppm)	Na (ppm)	K (ppm)	pH	Elevation (m)	Latitude	Longitude	Area (m^2)
ANG	1.7	8.2	2.1	1.9	5.39**	2,600	37°38'24"N	107°47'45"W	8,800
SPR	0.4	2.5	1.6	0.4	5.96**	3,400	37°53'53"N	107°58'23"W	7,800
SLK	20.2	68.8	7.4	3.8	6.98	2,700	41°20'31"N	106°10'2"W	15,300
MBP	11.6	34.2	0.7	0.3	6.88	3,200	41°20'58"N	106°15'15"W	24,800

* Cation and pH estimates are means from two samples, one collected from each plant community, at each site during the growing season of 2013.

** Only one measurement was used from a 2006-2007 San Juan fen survey (Chimner *et al.* 2010).

Table 2.2. Climate and hydrological characteristics and growing season net ecosystem production at each site.

Site	Year	Date of peak* SWE	Peak SWE* (cm)	Date of melt -out	Growing season precip. (mm)	Mean growing season air temperature (°C)**	Mean growing season water table (cm)**	Mean growing season NEP (g CO_2-C m^{-2})***
							LAS, LUT	*LAS, LUT*
ANG	2012	3/4	32 (1.5)	4/5	124	15.4 (6.7)	-13.9 (8.8), -40.0 (16.5)	-25.4 (47.0), 17.7 (82.5)
	2013	3/10	30 (1.0)	4/21	224	14.9 (6.3)	-15.3 (6.9), -31.4 (16.6)	-43.0 (44.1), 31.6 (78.7)
							SAX, UTR	*SAX, UTR*
SPR	2012	3/21	48 (0.74)	5/15	124	10.5 (5.3)	-4.2 (12.7), -12.6 (3.4)	188.8 (74.5), 234.4 (58.3)
	2013	4/17	46 (0.84)	5/22	224	10.5 (5.4)	-3.8 (2.2), -6.2 (0.3)	188.2 (67.6), 256.2 (51.9)
							SIM and BET	*SIM, BET*
SLK	2012	2/23	34 (0.37)	3/31	63	13.0 (7.1)	-17.6 (9.7)	210.0 (66.2), 175.6 (54.5)
	2013	4/17	34 (0.37)	5/15	199	12.5 (6.9)	-52.0 (30.4)	-341.8 (167.2), -53.4 (127.8)
							AQU, PLA	*AQU, PLA*
MBP	2012	2/14	24 (0.38)	4/2	63	11.2 (5.8)	-24.1 (16.5), -12.4 (4.8)	70.7 (119.9), 237.8 (55.6)
	2013	4/17	48 (0.30)	6/1	199	10.7 (5.5)	-5.9 (3.7), -4.8 (1.3)	150.5 (977.4), 234.6 (53.6)

* See Chapter 2 for further details on peak SWE calculations. Values are means with standard deviation of the posterior estimates in parentheses.

** Values in parentheses represent standard deviation.

*** Values in parentheses represent standard deviation of the posterior mean.

0

Table 2.3. Gross primary production and ecosystem respiration model parameter estimates.

	ANG-LAS	ANG-LUT	SPR-SAX	SPR-UTR
A_{max}	0.57 (0.13)	0.57 (0.13)	1.40 (0.46)	1.24 (0.59)
α	0.0018(0.00097)	0.011 (0.0062)	0.0030 (0.0012)	0.0070 (0.0054)
RAV_{optGPP}	23.8 (3.9)	24.4 (3.8)	23.2 (4.5)	22.8 (4.9)
RAV_{devGPP}	10.5 (2.4)	12.0 (3.3)	10.6 (2.2)	10.3 (3.0)
σ_{GPP}	0.40 (0.038)	0.67 (0.066)	0.52 (0.047)	0.85 (0.014)
N	78	69	73	69
R^2	0.65	0.49	0.72	0.61
Q_{10}	1.2 (0.088)	1.3 (0.099)	1.5 (0.30)	1.2 (0.14)
R_{10}	0.14 (0.032)	0.15 (0.035)	0.14 (0.051)	0.15 (0.051)
b	0.0069 (0.0037)	0.003 (0.0023)	0.016 (0.01)	0.012 (0.0062)
RAV_{optER}	21.4 (4.4)	19.7 (4.7)	19.8 (6.5)	21.0 (5.9)
RAV_{devER}	10.3 (3.6)	10.8 (5.6)	17.7 (6.2)	15.4 (5.8)
σ_{ER}	0.12 (0.13)	0.22 (0.025)	0.25 (0.027)	0.13 (0.014)
N	58	53	49	52
R^2	0.74	0.75	0.32	0.30

	SLK-SIM	SLK-BET	MBP-AQU	MBP-PLA
A_{max}	1.32 (0.29)	1.24 (0.25)	1.35 (0.38)	1.59 (0.49)
α	0.0021 (0.00057)	0.0022 (0.00062)	0.0027 (0.00084)	0.0035 (0.0012)
RAV_{optGPP}	22.9 (4.1)	24.0 (3.7)	23.2 (4.5)	21.9 (4.9)
RAV_{devGPP}	10.8 (2.0)	11.3 (1.9)	12.3 (2.6)	10.3 (2.4)
σ_{GPP}	0.68 (0.056)	0.66 (0.053)	0.86 (0.077)	1.1 (0.09)
N	97	101	85	88
R^2	0.80	0.80	0.72	0.75
Q_{10}	1.5 (0.2)	1.3 (0.096)	1.2 (0.15)	1.2 (0.075)
R_{10}	0.12 (0.032)	0.15 (0.030)	0.17 (0.038)	0.19 (0.032)
b	0.019 (0.0024)	0.0095 (0.0028)	0.012 (0.0058)	0.04 (0.0072)
RAV_{optER}	24.4 (3.9)	24.2 (4.0)	18.7 (6.7)	21.6 (5.2)
RAV_{devER}	18.0 (3.9)	18.8 (4.1)	19.7 (5.9)	17.5 (5.1)
σ_{ER}	0.15 (0.014)	0.16 (0.014)	0.25 (0.027)	0.15 (0.016)
N	71	75	52	51
R^2	0.67	0.58	0.30	0.75

Values in parentheses represent the standard deviation for the posterior means.

Table 2.4. Mean parameter estimates for the BMLR model.

	Parameter estimate*
β_0	438.7 (175.8)
β_1	-16.7 (15.2)
β_2	7.0 (1.9)
$\sigma_{procNEP}$	103.9 (22.2)

* Values in parentheses represent standard deviation.

References

Adkinson AC, Syed KH, Flanagan LB (2011) Contrasting responses of growing season ecosystem CO 2 exchange to variation in temperature and water table depth in two peatlands in northern Alberta, Canada. *Journal of Geophysical Research*, **116**, 1–17.

Ashfaq M, Ghosh S, Kao S-C *et al.* (2013) Near-term acceleration of hydroclimatic change in the western U.S. *Journal of Geophysical Research: Atmospheres*, **118**, 10,676–10,693.

Aurela M (2002) Annual CO_2 balance of a subarctic fen in northern Europe: Importance of the wintertime efflux. *Journal of Geophysical Research*, **107**, 4607.

Beniston M (2003) Climate change in mountain regions: A review of possible impacts. *Climatic Change*, **59**, 5–31.

Blanken PD (2014) The effect of winter drought on evaporation from a high-elevation wetland. 1354–1369.

Bubier JL, Bhatia G, Moore TR, Roulet NT, Lafleur PM (2003) Spatial and temporal variability in growing-season net ecosystem carbon dioxide exchange at a large peatland in Ontario, Canada. *Ecosystems*, **6**, 353–367.

Chapin AFS, Woodwell GM, Randerson JT *et al.* (2006) Reconciling Carbon-cycle Concepts, Terminology, and Methods. **9**, 1041–1050.

Chimner RA, Cooper DJ (2003a) Influence of water table levels on CO_2 emissions in a Colorado subalpine fen: an in situ microcosm study. *Soil Biology and Biochemistry*, **35**, 345–351.

Chimner RA, Cooper DJ (2003b) Carbon dynamics of pristine and hydrologically modified fens in the southern Rocky Mountains. *Canadian Journal of Botany*, **81**, 477–491.

Chimner RA, Cooper DJ, Parton WJ (2002) Modeling carbon accumulation in Rocky Mountain fens. **22**, 100–110.

Chimner RA, Lemly JM, Cooper DJ (2010) Mountain Fen Distribution, Types and Restoration Priorities, San Juan Mountains, Colorado, USA. *Wetlands*, **30**, 763–771.

Christensen NS, Lettenmaier DP (2007) A multimodel ensemble approach to assessment of climate change impacts on the hydrology and water resources of the Colorado River Basin. *Hydrology and Earth System Sciences*, **11**, 1417–1434.

Christensen NS, Wood AW, Voisin N, Lettenmaier DP, Palmer RN (2004) The effects of climat change on the hydrology and water resources of the Colorado River Basin. *Climatic Change*, **62**, 337–363.

Cooper DJ (1996) Water and soil chemistry, floristics, and phytosociology of the extreme rich High Creek fen, in South Park, Colorado3 U.S.A. *Canadian Journal of Botany*, **74**, 1801–1811.

Cooper DJ, Wolf EC, Ronayne MJ, Roche JW (2015) Effects of groundwater pumping on the sustainability of a mountain wetland complex, Yosemite National Park, California. *Journal of Hydrology: Regional Studies*, **3**, 87–105.

Gelman A, Rubin DB (1992) Inference from iterative simulation using multiple sequences. *Statistical Science*, **7**, 457–511.

Gorham E (1991) Northern peatlands: Role in the carbon cycle and and probable response to climatic warming. *Ecological Applications*, **1**, 182–195.

Heidel B, Jones G (2006) *Botanical and Ecological Characteristics of Fens in the Medicine Bow Mountains , Medicine Bow National Forest Albany and Carbon Counties , Wyoming*. Wyoming Natural Diversity Database, University of Wyoming.

Johnson CP, Pypker TG, Hribljan JA, Chimner RA (2013) Open Top Chambers and Infrared Lamps: A Comparison of Heating Efficacy and CO2/CH4 Dynamics in a Northern Michigan Peatland. *Ecosystems*, **16**, 736–748.

Krajick K (2004) All Downhill from Here ? *Science*, **303**, 1600–1602.

Letts MG, Roulet NT, Comer NT, Skarupa MR, Verseghy DL (2000) Parametrization of peatland hydraulic properties for the Canadian land surface scheme. *Atmosphere-Ocean*, **38**, 141–160.

Maanavilja L, Riutta T, Aurela M, Pulkkinen M, Laurila T, Tuittila E-S (2011) Spatial variation in CO2 exchange at a northern aapa mire. *Biogeochemistry*, **104**, 325–345.

Moore C, Kampf S, Stone B, Richer E (2014) A GIS-based method for defining snow zones: application to the western United States. *Geocarto International*, **30**, 62–81.

Parmesan C (2006) Ecological and Evolutionary Responses to Recent Climate Change. *Annual Review of Ecology, Evolution, and Systematics*, **37**, 637–669.

Patterson L, Cooper DJ (2007) The use of hydrologic and ecological indicators for the restoration of drainage ditches and water diversions in a mountain fen, Cascade Range, California. *Wetlands*, **27**, 290–304.

Regonda SK, Rajagopalan B, Clark M, Pitlick J (2004) Seasonal Cycle Shifts in Hydroclimatology over the Western United States. *Journal of Climate*, **18**, 372–384.

Riutta T, Laine J, Tuittila E-S (2007) Sensitivity of CO2 Exchange of Fen Ecosystem Components to Water Level Variation. *Ecosystems*, **10**, 718–733.

Rood SB, Pan J, Gill KM, Franks CG, Samuelson GM, Shepherd A (2008) Declining summer flows of Rocky Mountain rivers: Changing seasonal hydrology and probable impacts on floodplain forests. *Journal of Hydrology*, **349**, 397–410.

Schimelpfenig DW, Cooper DJ, Chimner RA (2013) Effectiveness of Ditch Blockage for Restoring Hydrologic and Soil Processes in Mountain Peatlands. *Restoration Ecology*, n/a–n/a.

Sullivan PF, Arens SJT, Chimner RA, Welker JM (2007) Temperature and Microtopography Interact to Control Carbon Cycling in a High Arctic Fen. *Ecosystems*, **11**, 61–76.

Tufford DL (2011) Shallow water table response to seasonal and interannual climate variability. *Advances in Forest Hydrology*, **54**, 2079–2086.

Vidon P (2012) Towards a better understanding of riparian zone water table response to precipitation: surface water infiltration, hillslope contribution or pressure wave processes? *Hydrological Processes*, **26**, 3207–3215.

Warshall P (1994) The Madrean Sky Island Archipelago : A Planetary Overview. In: *Biodiversity and Management of the Madrean Archipelago: The Sky Islands of Southwestern United States and Northwestern Mexico* (ed De Bano LF, Ffolliott PF O-RA), pp. 6–18. US Department of Agriculture, Fort Collins, Colorado.

Wohlfahrt G, Cremonese E, Hammerle A *et al.* (2013) Tradeoffs between global warming and day length on the start of the carbon uptake period in seasonally cold ecosystems. *Geophysical research letters*, **40**, 6136–6142.

Wu J, Roulet NT, Sagerfors J, Nilsson MB (2013) Simulation of six years of carbon fluxes for a sedge-dominated oligotrophic minerogenic peatland in Northern Sweden using the McGill Wetland Model (MWM). *Journal of Geophysical Research: Biogeosciences*, **118**, 795–807.

3 Effects of climate regime on groundwater recharge and hydrological dynamics in mountain fens

3.1 Introduction

One of the most important ecohydrological characteristics of wetland ecosystems is the presence of saturated soils. A water table (WT) near the soil surface creates an interaction of groundwater flow with a biologically active zone where plants and soil microbes dominate biogeochemical processes under anaerobic conditions. These conditions contribute to the critical ecological services provided by wetlands, including the removal of groundwater contaminants before they reach surface waters (Kellogg *et al.*, 2009) and sequestering of carbon (C) from the atmosphere (Gorham, 1991). Further, the water-logged soil conditions found in wetlands exert a strong control on plant production and community composition (Dwire *et al.*, 2006; Wolfe *et al.*, 2006), and therefore contribute greatly to the conservation value of these ecosystems. Near-surface water tables are particularly important in mountain peatlands, where they play a critical role in sustaining organic soils (Chimner and Cooper, 2003a; Schimelpfenig et al., 2013) and the unique vegetation found in these ecosystems (Cooper & Andrus, 1994).

In the western US, groundwater-fed peatlands known as fens exist at high elevations in the Cascade, Sierra Nevada, and Rocky Mountains (Cooper et al. 2012). These ecosystems provide important refugia for regionally rare plant species typically found in boreal regions (Chimner *et al.*, 2010), serve as locally important C sinks (Chimner and Cooper, 2003b), and act as important regulators of groundwater flow, as they are typically positioned at focal points for groundwater and surface water flow on the landscape (Winter, 1999). The majority of precipitation in mountain regions of the western US falls during the winter and spring as snow and accounts for the majority of precipitation that sustains hydrological inputs to mountain

wetlands (Woods *et al.*, 2006). In the Sierra Nevada and most of the Rocky Mountains, relatively little precipitation falls during the growing season. However, southern portions of the Rocky Mountains receive late-summer precipitation driven by the North American Monsoon, with significantly greater rainfall than areas further north (Mahmood & Vivoni, 2014). Such differences in late-summer precipitation regime may differentially affect WT dynamics in fens of the Rocky Mountains that are located at different latitudes. Because the WT occurs within the root zone of phreatophytes, mountain fens also play a unique role in groundwater flow dynamics, as groundwater is removed from the system via evapotranspiration (ET). Consequently, evapotranspiration demands on groundwater also exert a strong control on WT position (Fahle & Dietrich, 2014).

In the past several decades, a warming climate in mountain regions of the western US has impacted hydrological cycles. Mountain peatlands are typically small, relative to peatlands in boreal regions, due to steep slopes and valley confinement (Patterson & Cooper, 2007) and therefore may be more susceptible to climate-driven changes in groundwater dynamics than peatlands occurring in larger groundwater flow systems (Kløve *et al.*, 2014). Increases in air temperature have led to reductions in peak snow packs and earlier melting, with more winter precipitation falling as rain instead of snow (Regonda *et al.*, 2004; Christensen & Lettenmaier, 2007). This shift in the timing of important hydrological processes has reduced late-summer stream flows and led to drought stress in riparian ecosystems (Hamlet *et al.*, 2005; Rood *et al.*, 2008; Clow, 2010). Similarly, changes in snowmelt dynamics and their ultimate effect on groundwater recharge may lead to reduced WT positions in mountain fens during the growing season. In addition, increases in air temperatures and longer growing seasons have been

associated with increased wetland ET and a subsequent decrease in WT during the growing season (Roulet *et al.,* 1992; Bridgham *et al.,* 1999; Riutta *et al.,* 2007).

Peatlands are defined by the presence of organic soils that form as a result of decomposition being limited by anaerobic soil conditions. Therefore, maintaining a water table near the soil surface is critical for the ecological functioning and sustainability of peatlands. If water tables are lowered due to climate change or other anthropogenic disturbances, increased ecosystem respiration can occur and they can shift from being C sinks to sources (Chimner and Cooper, 2003a; Riutta et al., 2007; Wu et al., 2013). Additionally, declines in water tables have been associated with shifts in plant species composition in mountain fens of the western US (Bartolome et al. 1990). In order to better understand the effects of climate change on groundwater dependent ecosystems, there is a need for more detailed information on the mechanisms of groundwater recharge, particularly for mountain fens founds in cold and alpine environments (Kløve *et al.,* 2014).

Recent studies have highlighted the utility of telemetric snow course data along with snow depth in modeling dynamics in snow water equivalent (SWE) (McCreight & Small, 2014; Parida & Buermann, 2014), which can be monitored using automated cameras (Parajka *et al.*, 2012). This allows for modeling melted snow available for groundwater recharge on a daily time step during snowmelt. In addition, the relationship between ET and WT can be utilized in developing models of groundwater flow, using diurnal changes in WT along with meteorological data, to estimate ET losses from the saturated zone (Loheide, 2008; Carlson Mazur *et al.*, 2013). In this study, I used these methods to model hydrological dynamics that control WT position during snowmelt as well as the growing season in high and low elevation fens occurring in regions with differing monsoon influence. My objectives were to i) examine differences in the

peak SWE, timing of snowmelt, and subsequent WT dynamics in fens occurring at high and low elevations at different latitudes and ii) to compare growing season WT dynamics in response to varying ET and precipitation regimes at two low elevation fens.

3.2 Methods

Study sites

This study investigated four fens in the Rocky Mountains, two in the San Juan Mountains of southwestern Colorado and two in the Medicine Bow Mountains of southern Wyoming (Table 3.1). To capture water table dynamics during snow melt under high and low peak SWE within each region, fens were selected at the high and low end of their known elevation ranges (Chimner et al. 2010, Heidel and Jones 2006). Anglica Fen (ANG), the low elevation fen in the San Juan Mountains, occupies a basin consisting of fractured bedrock, with no major surface water inflows or outflows. Spruce Fen (SPR) is the high elevation site in the same region and occurs on a gentle slope, with a surface water inlet and outlet that flow throughout the growing season. In the Medicine Bow Mountains, the low elevation site, Sand Lake Fen (SLK), is a gently sloping peatland with no major surface water inflows or outflows. Medicine Bow Peak Fen (MBP), which served as the high elevation site in the Medicine Bow Mountains, is a sloping fen with a groundwater discharge point at its upgradient end, and a small area of surface water at its downgradient end. See Chapter 1 for descriptions of fen plant community compositions.

Snow water equivalent model

Field Measurements

Water table position was measured and logged on an hourly basis in a centrally located monitoring well in each fen using an In-Situ Rugged Troll (Fort Collins, CO) down-well

pressure transducer throughout 2012 and 2013. Snow depth at each site was measured and logged on a daily basis using a snow stake and an on-site automated digital camera (Moultrie Gamespy). Snow stakes consisted of 2.54-cm diameter PVC pipe, approximately 3 m long, marked at 5-cm increments. At each site, the camera was pointed at the stakes and set to take a photograph each day at 12:00. I also obtained measurements of snow depth and SWE recorded at nearby SNOTEL sites at similar elevations. These measurements were used to correlate changes in snow depth between SNOTEL sites and study fens, as well as model the relationship between SWE and snow depth during snowmelt.

Model description

SWE and snow depth data collected at SNOTEL sites were combined for both study years to parameterize the model of SWE as a function of depth. However, due to dissimilarities between snowmelt and WT dynamics between years at each site, models of WT position as a function of SWE melt were parameterized individually for each year. For each SNOTEL site, 2nd order polynomial functions, with y-intercepts set at zero, were used to model SWE as a function of snow depth in 2012 and 2013 (Equation 1). Daily SWE and snow depth data from the date of peak SWE until complete melt-out were used to fit models.

$$\boldsymbol{SWE_{SNOTEL} = a * snow\ depth^2_{SNOTEL} + b * snow\ depth_{SNOTEL}} \quad \textbf{(1)}$$

Once parameters were estimated for SWE vs depth at the SNOTEL site, they were incorporated into a hierarchical model for each site, where daily SWE was modeled as a function of snow depth during the time period between peak SWE and complete snowmelt (Equation 2).

$$\boldsymbol{SWE_{fen(modeled)} = a * snow\ depth_{fen}^2 + b * snow\ depth_{fen}} \quad \textbf{(2)}$$

Snow water equivalent model development and evaluation

Models were fit to the measured data using Bayesian methods in R statistical software. Model parameters were estimated using Markov chain Monte Carlo (MCMC) analysis in the *rjags* package for R (Plummer, 2011). At least 200,000 iterations were used with 3 MCMC chains, with burn-in after 100,000 iterations. Vague priors were used for all model parameters. Normal distributions were used for all priors.

$$\boldsymbol{SWE_i^{obs} \sim Normal(\mu SWE_i, \sigma_{procSWE})} \quad \textbf{(3)}$$

Equation 3 represent the likelihood function for the observed SWE (SWE_i^{obs}) for each SNOTEL site. In the equations, μSWE_i represent the predicted values SWE, and $\sigma_{procSWE}$ represents the process variance associated with those predictions. Convergence was ensured for all parameter estimates and model predictions using the Gelman-Rubin diagnostic (Gelman and Rubin 1992) (Table 3.2).

Growing season water budget model

Field measurements

Growing season hydrological field measurements were carried out at both low elevation sites in 2012 and 2013. As with the snow water equivalent modeling, In-Situ Rugged Troll down-well pressure transducers were used to log WT position on an hourly basis at a centrally located monitoring well at each site. Adjacent to the monitoring well at each site, meteorological

station were installed which included a Hobo Onset RG-2 data logging rain gauges (Bourne, MA), and In-Situ Barotroll logging barometric pressure and air temperature sensor (Fort Collins, CO). Net radiation (R_{net}) and soil heat flux (G) were measured using Radiation Energy Balance net radiometers and soil heat flux plates (Seattle, WA). Net radiometers were installed 2 m above the fen surface, and soil heat flux plates were installed 5 cm below the peat surface, both of which were connected to a Campbell CR-10X (Logan, Utah) data logger in order to obtain hourly measurements.

Growing season water budget models

I developed models of growing season water budgets, run on hourly time steps, at the two low elevation fens in each region (ANG in the San Juan Mountains and SLK in the Medicine Bow Mountains) in 2012 and 2013, from June 1st through September 15th (Equation 4).

$$\boldsymbol{\Delta S = P - ET_G + GW_{net}} \quad \textbf{(4)}$$

In Equation 4, ΔS is the daily change in groundwater storage, P is the daily total precipitation, ET_G is the daily total ET losses from groundwater, and GW_{net} accounts for the daily net flow of groundwater. All estimates are in units of mm d^{-1}. Daily precipitation used in the models came directly from tipping bucket rain gauges. A simple equation that incorporates daily changes in WT position with an estimate of specific yield was used to model ΔS.

$$\boldsymbol{\Delta S = \Delta WT * S_y} \quad \textbf{(5)}$$

In Equation 5, ΔWT represents the daily net change in WT position, and S_y represents readily available specific yield. Readily available specific yield was estimated at each site as the ratio of infiltrated precipitation to rise in WT for rain events ≥ 5 mm. This method is appropriate for use in wetlands, where water tables are high, and a capillary fringe extends close to or at the soil surface (Rosenberry & Winter, 1997; Loheide *et al.*, 2005; Carlson Mazur *et al.*, 2013).

Methods used in modeling ET_G based on diurnal WT fluctuations require time periods without precipitation, which can confound modeling efforts (Carlson Mazur *et al.*, 2013). In order to model ET_G throughout the growing season, including periods of time where WT positions were affected by precipitation events, a multiple linear regression model was developed using a 21-day running average of air temperature (RAV) and potential evapotranspiration (PET) as predictor variables (Equation 6). Incorporating RAV as a predictor variable in the ET_G model allows for changes in plant phenology, which more accurately reflected seasonal variation in ET_G fluxes (i.e. as plants increase in biomass as the season progresses, so do their ET demands).

$$\boldsymbol{ET_G = \beta_0 + \beta_1 PET + \beta_2 RAV} \quad \textbf{(6)}$$

For both sites during both growing seasons, at least 21 consecutive days with ≤ 0.2 mm of precipitation occurred during June. Therefore, I used diurnal WT fluctuations during these time periods to calibrate ET_G models. Throughout each growing season at each site, PET was modeled using the Priestley-Taylor method (Priestley and Taylor 1972). To improve estimates of PET based on regional climate conditions, Priestley-Taylor coefficients (α) of 2.01 and 1.92 were used for ANG and SLK, respectively (Cristea *et al.*, 2013). Due to data logger malfunction, R_{net} and G were not recorded at SLK from 6/25/12 to 7/8/12. Average daily PET, using

measurements collected 5 days before and 5 days after the data logger malfunction, were used to fill the gap in PET data.

Because diurnal WT dynamics varied between sites, two different modeling approaches were used in estimating ET_G (Figure 3.1). Strong diurnal oscillations in WT position were apparent during both growing seasons at SLK, with a drop in position during the day as a result of ET demands, and a rise during the night as a result groundwater flow from a recovery source. Therefore, I used methods described by Loheide 2008 for modeling hourly rates of ET_G at SLK, which are applicable for a diurnally oscillating WT while accounting for longer term trends in WT position.

$$\boldsymbol{ET_G = GW_{rec} - S_y * \frac{dWT}{dt}} \quad \textbf{(7)}$$

Using the methods of Loheide 2008, it was assumed that the overall rate of change in head at the recovery source is equal to the rate of change in head at the monitoring well. A locally weighted regression (LOESS) smoothing function (span = 0.007) was used to filter out noise in the WT data (Carlson-Mazur et al. 2013, Cleveland 1979). For each day during the model calibration period, hourly WT measurements were detrended by subtracting the linear regression of the overall trend in water table position from the nighttime hours the day before and the day after being analyzed. Once the WT was detrended, another linear regression was made, regressing the rate of change in detrended WT with the position of the detrended WT from 0:00 to 6:00 the nights before and after each day being analyzed. This regression was then retrended and multiplied by S_y, which provides an estimate of GW_{rec}. Once GW_{rec} was known,

hourly ET_G rates were calculated using Equation 7, and summed every 24 hours to estimate daily fluxes.

At ANG, WT position decreased during the day, but to a lesser degree than SLK, and remained flat throughout the night. Since the rate of change in detrended WT from 0:00 to 6:00 was essentially zero throughout the calibration period at ANG (average slope = -0.02 cm hr^{-1}), GW_{rec} was set equal to zero in Equation 7. Daily ET_G was then calculated by multiplying S_y by the overall daily change in WT position.

For each day during the growing season, GW_{net} was determined by taking the net difference between the total inputs and outputs in Equation 4.

Growing season model development and evaluation

As with the snow water equivalent model, I fit growing season models to the measured data using Bayesian methods and model parameters were estimated using MCMC. A total of 25,000 iterations were used with 4 MCMC chains, with burn-in after 10,000 iterations. Vague priors were used for all model parameters. Normal distributions were used for all priors except for S_y, for which a beta distribution was used.

$$\boldsymbol{ETG_i^{obs} \sim Normal(\mu ETG_i, \sigma_{procETG})} \quad \textbf{(8)}$$

$$\boldsymbol{\Delta S_i^{obs} \sim Normal(\mu \Delta S_i, \sigma_{proc\Delta S})} \quad \textbf{(9)}$$

Equations 8 and 9 represent the likelihood functions for the observed ETG (ETG_i^{obs}) and ΔS (ΔS_i^{obs}) for each fen. In the equations, μETG_i and $\mu \Delta S_i$ represent the predicted values of ETG

and ΔS, respectively, and $\sigma_{proc\Delta S}$ and $\sigma_{proc\Delta S}$ represent the process variance associated with those predictions. Convergence was ensured for all parameter estimates and model predictions using the Gelman-Rubin diagnostic (Gelman and Rubin 1992) (Table 3.3). Daily and monthly ΔS, ET_G, and GW_{net} were estimated using MCMC, with a total of 6,000 iterations and burn-in at 3,000 iterations.

3.3 Results

Modeling snow water equivalent

Changes in snow depth during snowmelt at each study fen correlated well with nearby SNOTEL sites ($0.57 \leq R^2 \leq 0.97$). However, changes in snow depth between study fens and SNOTEL sites were more strongly correlated in the San Juan than the Medicine Bow Mountains (Figure 3.2). Models that predicted SWE as a function snow depth during snowmelt showed very strong correlation between these two variables ($0.96 \leq R^2 \leq 0.98$) at each of the SNOTEL sites, with process uncertainty ranging from 1.3 to 2.6 cm (Table 3.2, Figure 3.3).

Snowmelt and early growing season water tables

Peak SWE estimates were approximately 10 cm higher at high elevation versus low elevation sites, with the exception of MBP in 2012, which was lower than that all other estimates for all sites during both years (Figure 3.4). In the San Juan Mountains, peak SWE occurred approximately two weeks to over a month earlier at ANG than SPR. Correspondingly, ANG became snow-free approximately one month earlier than SPR during both study years. In the Medicine Bow Mountains, peak SWE was lowest at MBP in 2012, and highest in 2013. Unlike the San Juan Mountain sites, peak SWE at MBP occurred over three weeks earlier than at SLK in 2012, with both sites becoming snow-free only two days apart. In 2013, however, peak SWE at

both Medicine Bow Mountain sites occurred only three days apart, and SLK became snow-free approximately two weeks earlier than MBP.

Mean WT position for the month of June was lower at the low elevation fen during both study years, within each region. In addition, groundwater dynamics were less stable at both low elevation sites, with higher variance in WT position during this time period (Table 3.3).

Growing season water budgets

During the 2012 growing season, ANG received 124 mm of rainfall, most of which fell during July and August (Figure 3.5). During the same year, SLK received almost half this precipitation amount, 63 cm, of which the majority fell during the same months as ANG. Similarly, during the growing season of 2013 from June through August, approximately twice as much precipitation fell at ANG than SLK, 139 compared to 72 mm. However, unusually high precipitation during September at both sites, but more so for SLK, brought growing season total precipitation to similar amounts at both sites, 205 and 192 mm, for ANG and SLK, respectively.

Both sites had a decline in ΔS early in the growing season, with negative estimates for June during both years (Figure 3.5). From July through August of 2012, ANG had more modest declines in ΔS, while SLK had an increase over the same time period, with minimal changes during September of the same year for both sites. In July of 2013, ΔS at SLK had a similar decline as in June of the same year, followed by substantial increases in August and September. At ANG during the same year, minimal changes in ΔS occurred from July through August at ANG, and was followed by an increase in September. Mean posterior estimates of S_y used in calculating ΔS varied significantly between sites, 6.7×10^{-2} and 0.14 at SLK and ANG, respective (Table 3.4).

At each site, ET_G and GW_{net} followed similar seasonal patterns during both study years, however they were quite different between sites (Figure 3.5). Total growing season ET_G fluxes were over six times greater at SLK (630 – 674 mm) than ANG (89 – 90 mm). Similarly, growing season GW_{net} fluxes were strongly contrasting between sites, ranging from -132 to -73 mm at ANG, and 430 to 593 mm at SLK. At SLK, ET_G followed a parabolic pattern, exhibiting a gradual increase at the beginning of the growing season followed by a gradual decrease towards the end (Figures 3.6c and 3.6d). Monthly estimates of GW_{net} at SLK also followed a similar pattern as ET_G at this during both years (Figure 3.5). At ANG, however, ET_G showed a very gradual decline throughout the growing season, and GW_{net} remained negative throughout the growing season (Figures 3.6a and 3.6b).

Growing season water table dynamics

At both sites during both study years, WT position steadily declined during most of the month of June (Figures 3.6a-3.6d). Around the end of June, the downward trend in WT position begins to be punctuated with sharp rises, creating "spikes" in the hydrograph that coincide with rain events. These spikes were more frequent at ANG due to more frequent rain events during July and August. At SLK, spikes were less frequent in 2012 however they were often larger in magnitude than those of ANG. In late August of 2012, the rain gauge at SLK was knocked over by wildlife, and was not operational for approximately one week, which likely explains the absence of significant precipitation associated with the last major spike in the 2012. In 2013, the largest WT decline, to 99 cm below the peat surface, occurred in early August at SLK. This decline was followed by a rise in WT position to within 20 cm of the peat surface that coincided with the significant precipitation events of September 2013.

3.4 Discussion

Snowmelt and water table dynamics

My results show a trend of higher peak SWE and an approximately one month later onset of the snow-free season at the high elevation fens. Correspondingly, during both study years, WT position at the low elevation sites were lower in the early growing season following snowmelt than the high elevation sites. As snowmelt and thawing occurred earlier at the low elevation fens, it allowed for earlier onset of ET_G fluxes, and start of the growing season (Parida & Buermann, 2014). This likely contributed to the June declines in WT position at the low elevation fens.

The low SWE at MBP in 2012 was likely attributed to wind redistribution of snow at the site, which can be an important control on snowpack in mountain environments (Gauer, 2001). Further, snowfall records at the Brooklyn Lake SNOTEL site in the Medicine Bow Mountains revealed that the winter of 2011-12 saw the fourth smallest snowpack in the past 30 years, which was 67% of the long-term average and may have exacerbated the effects of the low peak SWE that year.

Growing season hydrological fluxes

Both ANG and SLK showed an overall decrease in calculated groundwater storage (negative ΔS) throughout both growing seasons, as driven by the decline in WT position apparent in the measured data. My estimates of S_y, a critical factor in calculating ΔS, varied substantially between sites, with posterior mean estimates about twice as high at ANG than at SLK. Both estimates, however, are within the range of readily available specific yield estimates reported for wetlands (Carlson Mazur *et al.*, 2013; Fahle & Dietrich, 2014), and the differences

in S_y between ANG and SLK may be due to differences in physical peat characteristics between the two sites associated with difference in vegetation (Lautz, 2008).

Both low elevation fens were characterized by major decreases in groundwater storage early in the year, with June having the most negative estimates of ΔS at both sites during both years, which coincided with steady WT declines. This was driven primarily by ET_G at both sites, as GW_{net} was always positive from June through August at SLK, and only slightly negative at ANG during June of both years. These results emphasize the importance of ET, being one of the largest outputs for a wetland water balance (Rosenberry *et al.*, 2004; Thompson *et al.*, 2014). The differing responses of GW_{net} between ANG and SLK highlight the importance of the hydrogeological setting in which they exist. For fens with a sufficiently large surrounding groundwater contributing area, such as SLK, groundwater baseflow will at least partially make up for water losses through daily ET_G demands, evident in the rising WT during nighttime hours. Alternatively, daily ET_G fluxes in basin fens surrounded by low permeability material, like ANG, will likely not be followed by WT rise at night, due to insufficient groundwater flow.

During both years, ET_G was an order of magnitude higher at SLK than at ANG. These differences in ET_G may have been driven by differences in plant transpiration driven by differences in aboveground biomass between the two sites, SLK being dominated by three woody species (*Salix planifolia*, *S. wolfii*, and *Betula glandulosa*) and a continuous sedge and moss carpet, while ANG was dominated by a sparse canopy of very thin leaved *Carex lasiocarpa* (Figure 3.7) (Bonfils *et al.*, 2012). Further, there was an extensive litter layer of sedge leaves and culms at ANG, visible in Figure 8, which could have further reduced ET_G by limiting soil evaporation (Mukherjee *et al.*, 2010; Balwinder-Singh *et al.*, 2011).

Roughly twice as much precipitation fell in July and August of both study years at ANG as at SLK, due to a stronger influence of the North American Monsoon in the San Juan Mountains. Rises in WT position occurred during all major rainfall events at both sites, but most often at ANG due to more frequent rain events. Water table position and ΔS typically peaked within approximately 48 hours following precipitation events at both sites. The delayed peak in WT position and ΔS coincided with peaks in GW_{net}, suggesting that rain events recharge groundwater in fen catchments, driving increases in flow to the center of the fens after a precipitation event has ceased (Stein *et al.*, 2004). A remarkable decrease in GW_{net} occurred late in the 2013 growing season at SLK, at the same time as record rainfall events occurred. Since our model assumes no surface water flow, this dramatic drop in GW_{net} is likely the result water leaving the fen as a major infiltration-excess overland flow event, uncharacteristic of peatlands under lesser rainfall intensities (Holden & Burt, 2002).

Implications of current hydrological dynamics and a future climate

This study identified a strong relationship between peak SWE and the WT position during the early stages of the growing season in mountain fens. I found that in low elevation fens, lower peak SWE resulted in lower WT positions than high-elevation fens, followed by a continued decline, punctuated by rises following rain events later in the summer. Temperatures are expected to increase and peak SWE is expected to decline by 10-40% at elevations similar to that of the low elevation fens (Christensen & Lettenmaier, 2007). It is possible that snowmelt and subsequent WT declines at these sites will occur earlier in the year. Such alterations in hydrological dynamics would lead to overall lower WT throughout the growing season, and potentially increase losses in soil C through increased ecosystem respirations (Chimner and

Cooper, 2003a; Schimelpfenig et al., 2013), particularly for fens located in regions with minimal monsoon preciptation. Such changes raise questions about the future sustainability of low elevation mountain fens, and also suggest that ecohydrological dynamics of higher elevation fens may become more similar to those found at lower elevations.

Table 3.1. Study fen location, elevation, size, and associated SNOTEL sites.

STUDY FENS					SNOTEL SITES		
	Elevation (m)	Latitude	Longitude	Area (m^2)	Site ID	Distance – direction from fen	Elevation (m)
Anglica Fen	2,600	37°38'24"N	107°47'45"W	8,800	Cascade #2 (# 387)	1 km – N	2,700
Spruce Fen	3,400	37°53'53"N	107°58'23"W	7,800	Red Mtn. Pass (#713)	11 km – SE	3,400
Sand Lake Fen	2,700	41°20'31"N	106°10'2"W	15,300	Cinnabar Park (#1046)	13 km – SW	2,900
Med. Bow Peak Fen	3,200	41°20'58"N	106°15'15"W	24,800	North French Creek (#668)	11 km – SW	3,100

Table 3.2. Snowmelt model parameter estimates.

Parameters	Anglica Fen	Spruce Fen	Sand Lake Fen	Medicine Bow Peak Fen
a	-1.3×10^{-3} (2.0×10^{-4})	-1.1×10^{-3} (1.1×10^{-4})	-1.6×10^{-3} (5.9×10^{-5})	-4.0×10^{-4} (5.0×10^{-5})
b	0.42 (0.014)	0.48 (0.013)	0.49 (8.1×10^{-3})	0.42 (7.3×10^{-3})
$\sigma_{procSWE}$	1.3 (0.13)	2.6 (0.21)	2.3 (0.17)	2.3 (0.16)

Table 3.3. Dates of peak snow water equivalent and beginning of the snow-free period, amount of peak SWE, and mean June WT position at each fen. For peak SWE, values in parentheses represent standard deviation of the posterior estimate. For WT, values in parentheses represent standard deviation of the monthly mean.

Site	Year	Date of peak SWE	Snow-free date	Peak SWE at fen (cm)	Mean June WT (cm)
Anglica Fen	2012	March 4th	April 5th	32 (1.5)	-5.7 (5.8)
	2013	March 10th	April 21st	30 (1.0)	-11.8 (6.6)
Spruce Fen	2012	March 21st	May 15th	48 (0.74)	2.9 (0.7)
	2013	April 17th	May 22nd	46 (0.84)	-6.5 (0.6)
Sand Lake Fen	2012	February 23rd	March 31st	34 (0.37)	-17.4 (11.9)
	2013	April 17th	May 15th	34 (0.37)	-26.9 (18.4)
Medicine Bow Peak Fen	2012	February 14th	April 2nd	24 (0.38)	-8.0 (5.2)
	2013	April 17th	June 1st	48 (0.30)	-8.1 (1.1)

Table 3.4. Growing season model parameter estimates.

Parameters	Anglica Fen	Sand Lake Fen
S_y	0.14 (1.7×10^{-2})	6.7×10^{-2} (1.3×10^{-2})
$\sigma_{procΔS}$	3.7(0.64)	4.2 (1.2)
β_0	0.17 (2.7×10^{-2})	-3.6×10^{-3} (0.13)
β_1	6.6×10^{-3} (2.0×10^{-2})	0.86 (6.4×10^{-2})
β_2	0.20 (0.29)	-4.8 (1.1)
$\sigma_{procETG}$	0.20 (2.1×10^{-2})	0.75 (8.0×10^{-2})

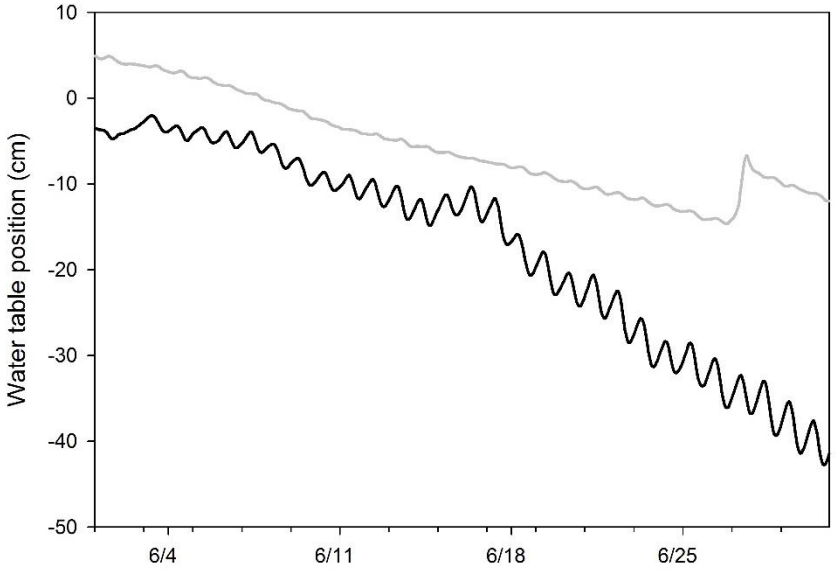

Figure 3.1. Differences in water table dynamics between Anglica Fen (grey) and Sand Lake Fen (black) during ET_G model calibration period in June of 2012.

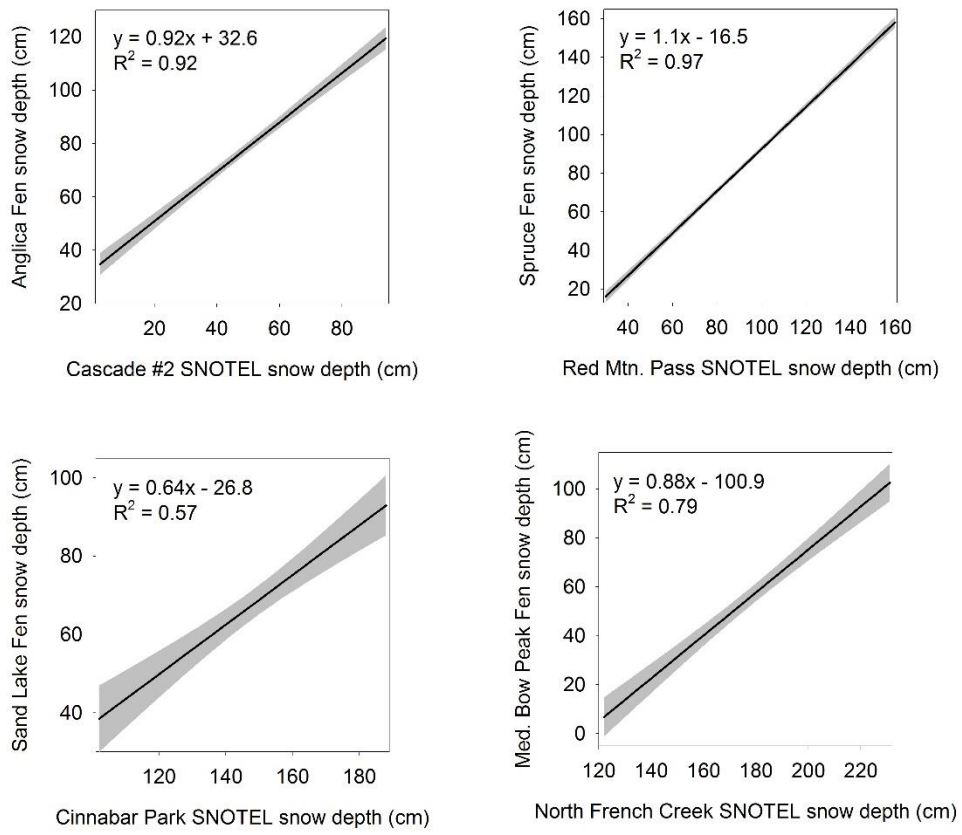

Figure 3.2. Modeled study fen snow depth versus measured snow depth at associated SNOTEL sites. Solid lines represent posterior mean estimates of snow depth at fen sites as a function of depth at associated SNOTEL sites during snow melt, and shaded regions represent the 95% credible limits.

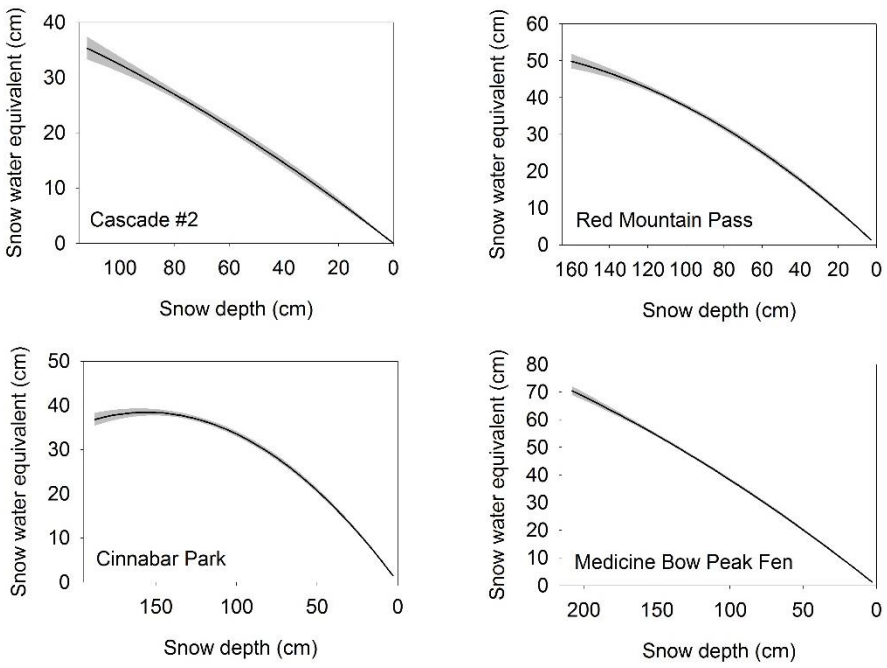

Figure 3.3. Modeled snow water equivalent (SWE) as a function of snow depth for each SNOTEL site. Solid lines represent posterior mean estimates of SWE as a function of snow depth during snow melt, and shaded regions represent the 95% credible limits.

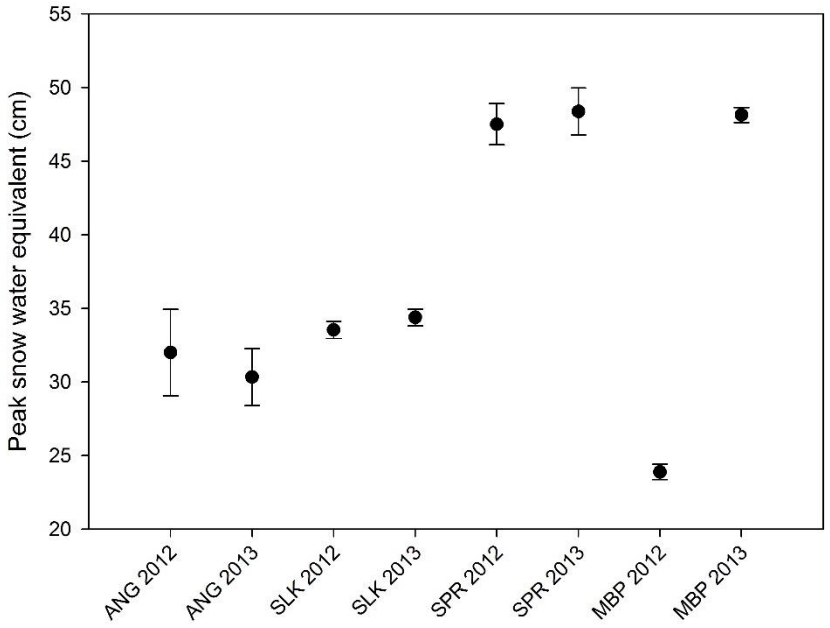

Figure 3.4. Posterior mean estimates of peak snow water equivalent for all study fens. Error bars represent upper and lower 95% credible limits.

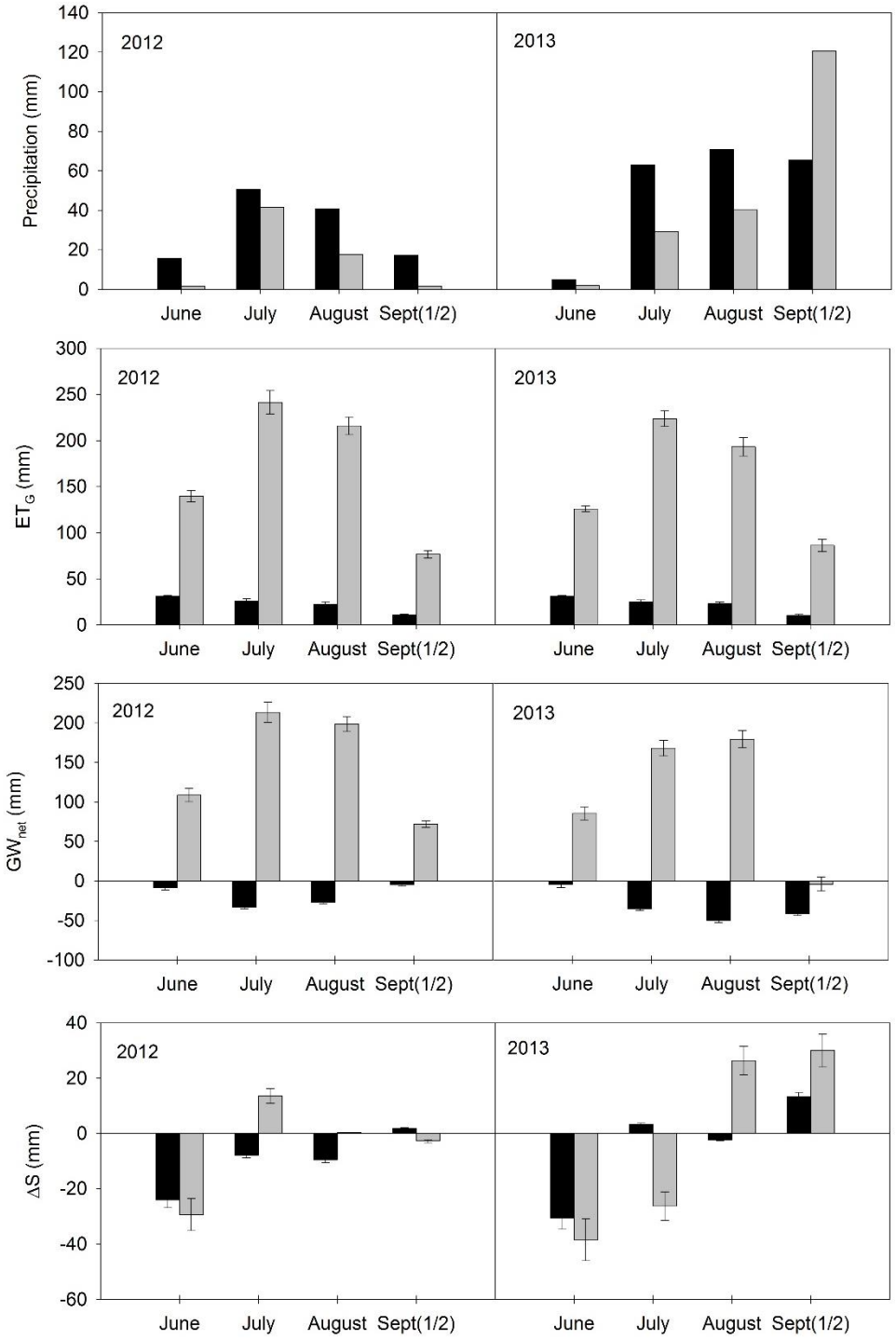

Figure 3.5. Monthly growing season water budget components for Anglica Fen (black) and Sand Lake Fen from June 1st through September 15th. For precipitation, bars represent monthly totals. For ET_G, GW_{net}, and ΔS, bars represent mean posterior estimates for monthly fluxes and error bars represent standard deviation of the posterior estimates.

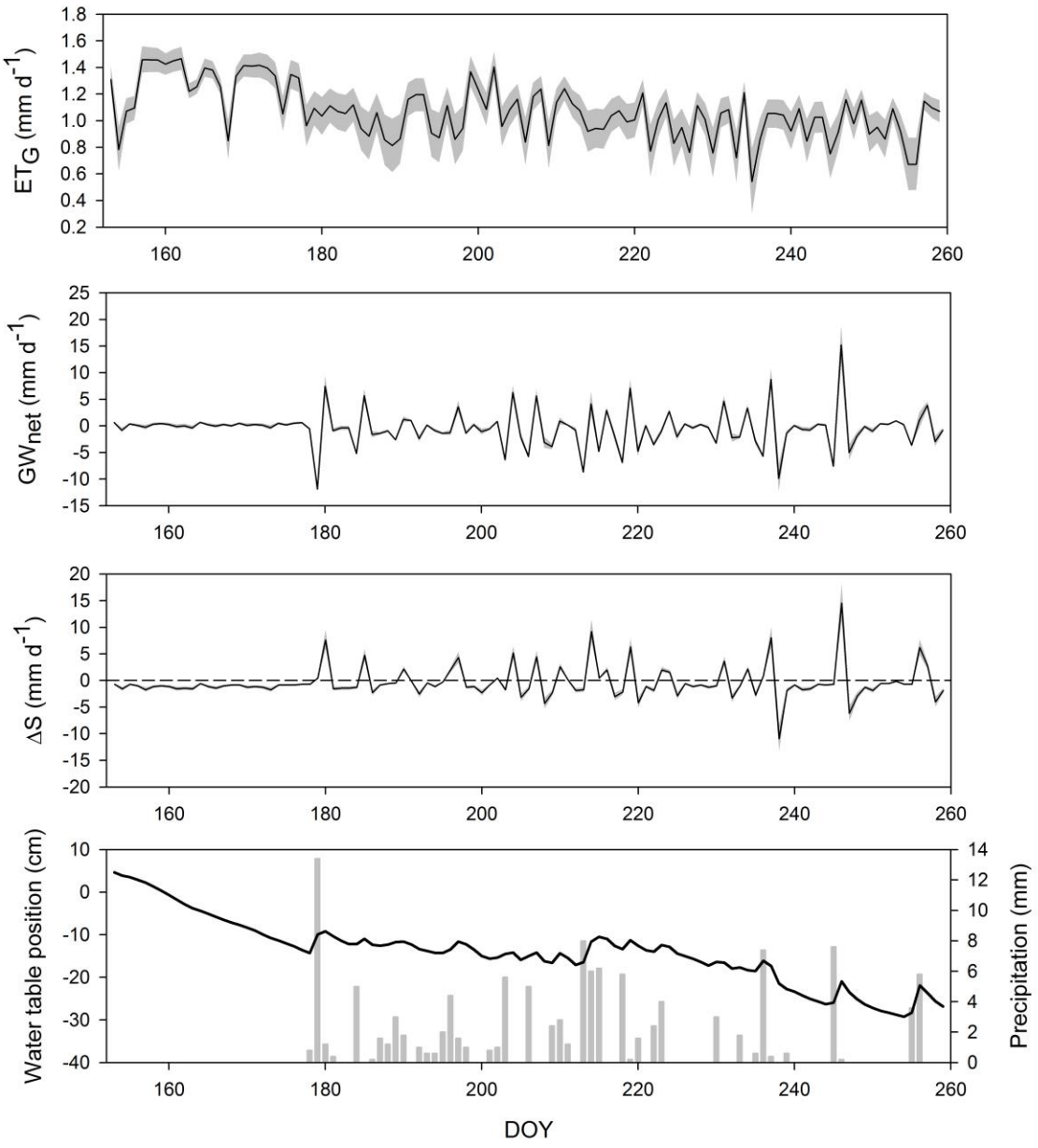

Figure 3.6a. Daily growing season water budget components for Anglica Fen in 2012. For ET_G, GW_{net}, and ΔS, solid black lines represent posterior mean estimates for daily fluxes and the shaded regions represent the 95% credible limits. Mean daily water table position is represented by a solid black line and daily total precipitation is represented by grey bars.

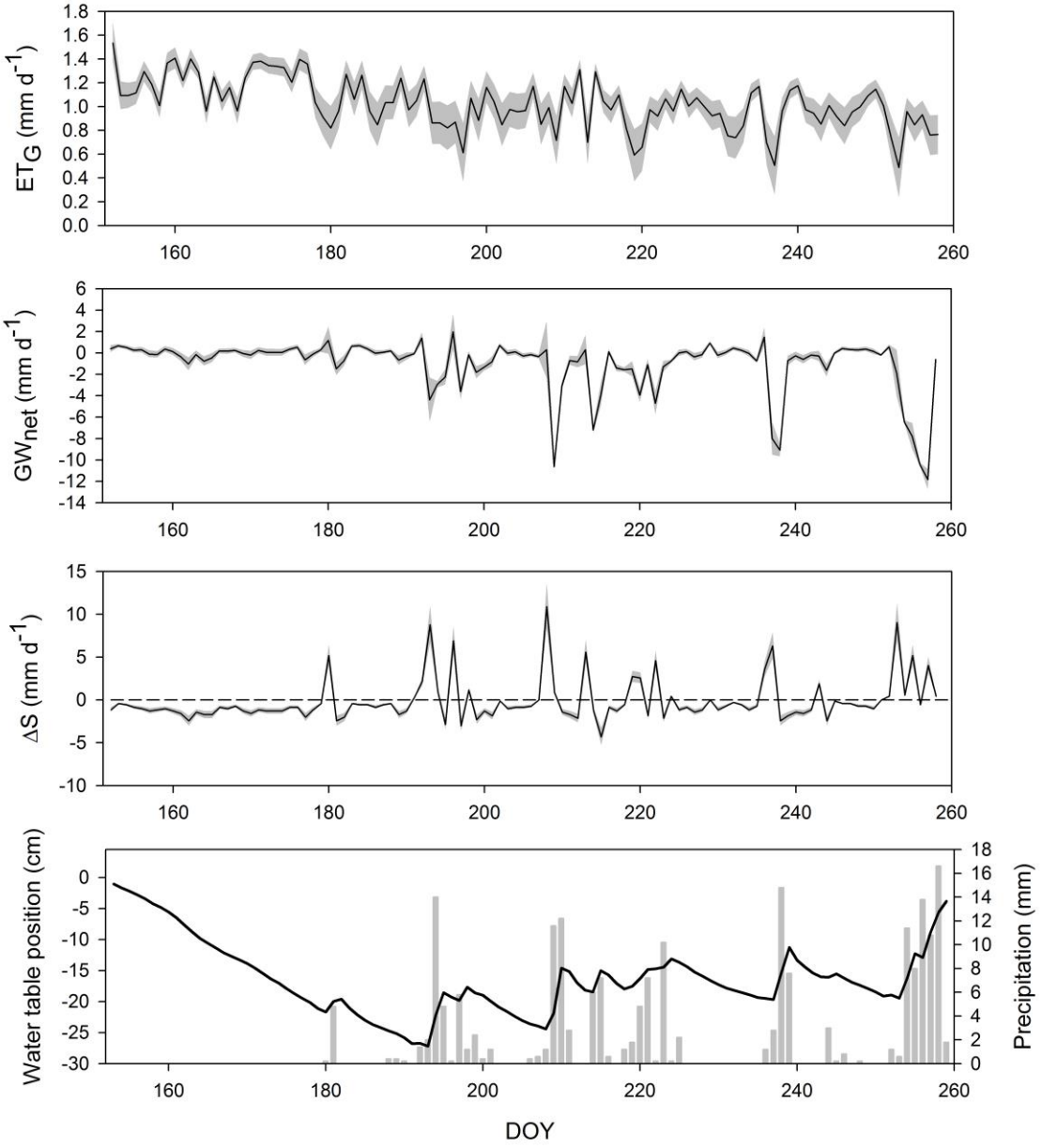

Figure 3.6b. Daily growing season water budget components for Anglica Fen in 2013. For ET_G, GW_{net}, and ΔS, solid black lines represent posterior mean estimates for daily fluxes and the shaded regions represent the 95% credible limits. Mean daily water table position is represented by a solid black line and daily total precipitation is represented by grey bars.

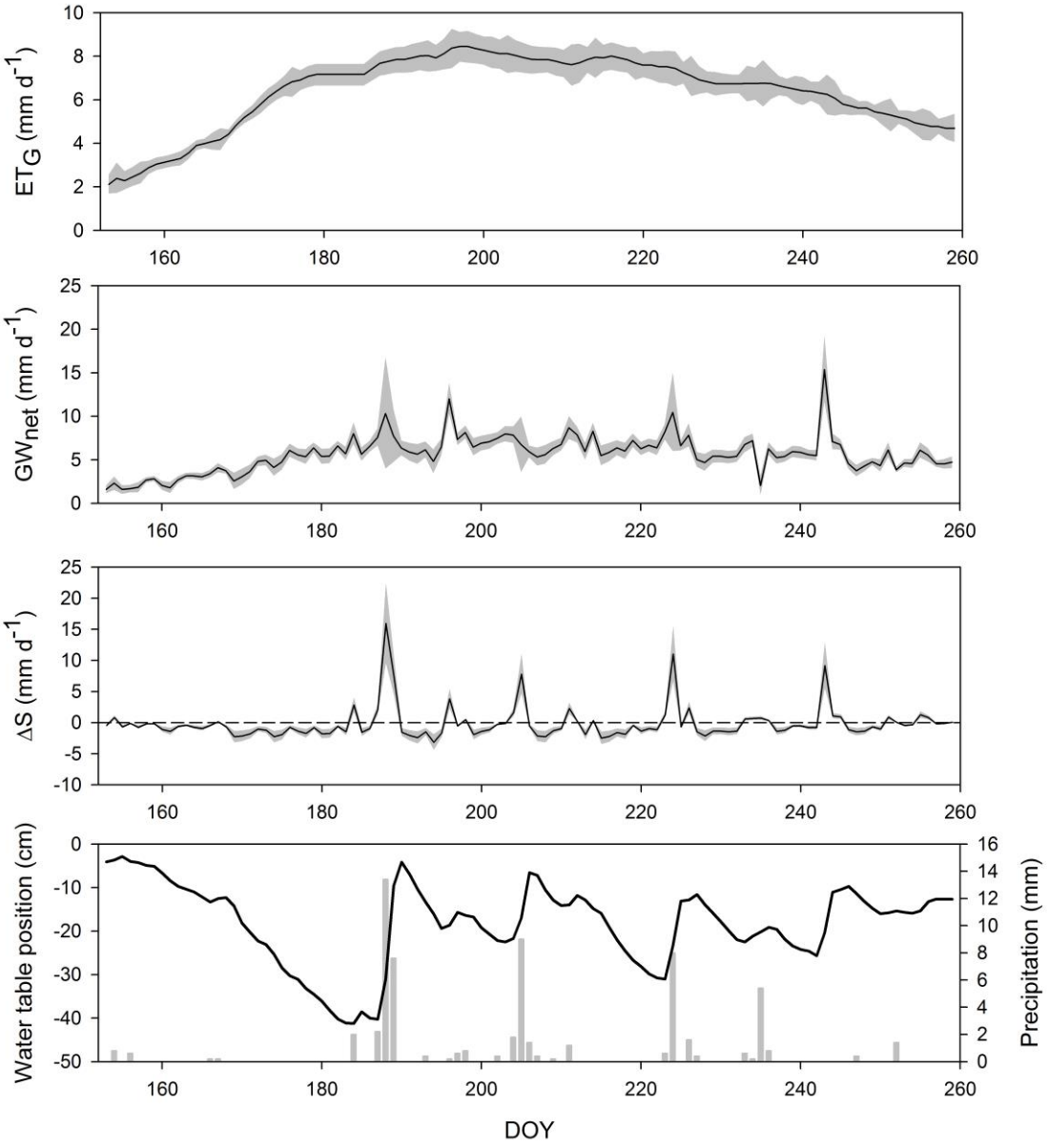

Figure 3.6c. Daily growing season water budget components for Sand Lake Fen in 2012. For ET_G, GW_{net}, and ΔS, solid black lines represent posterior mean estimates for daily fluxes and the shaded regions represent the 95% credible limits. Mean daily water table position is represented by a solid black line and daily total precipitation is represented by grey bars.

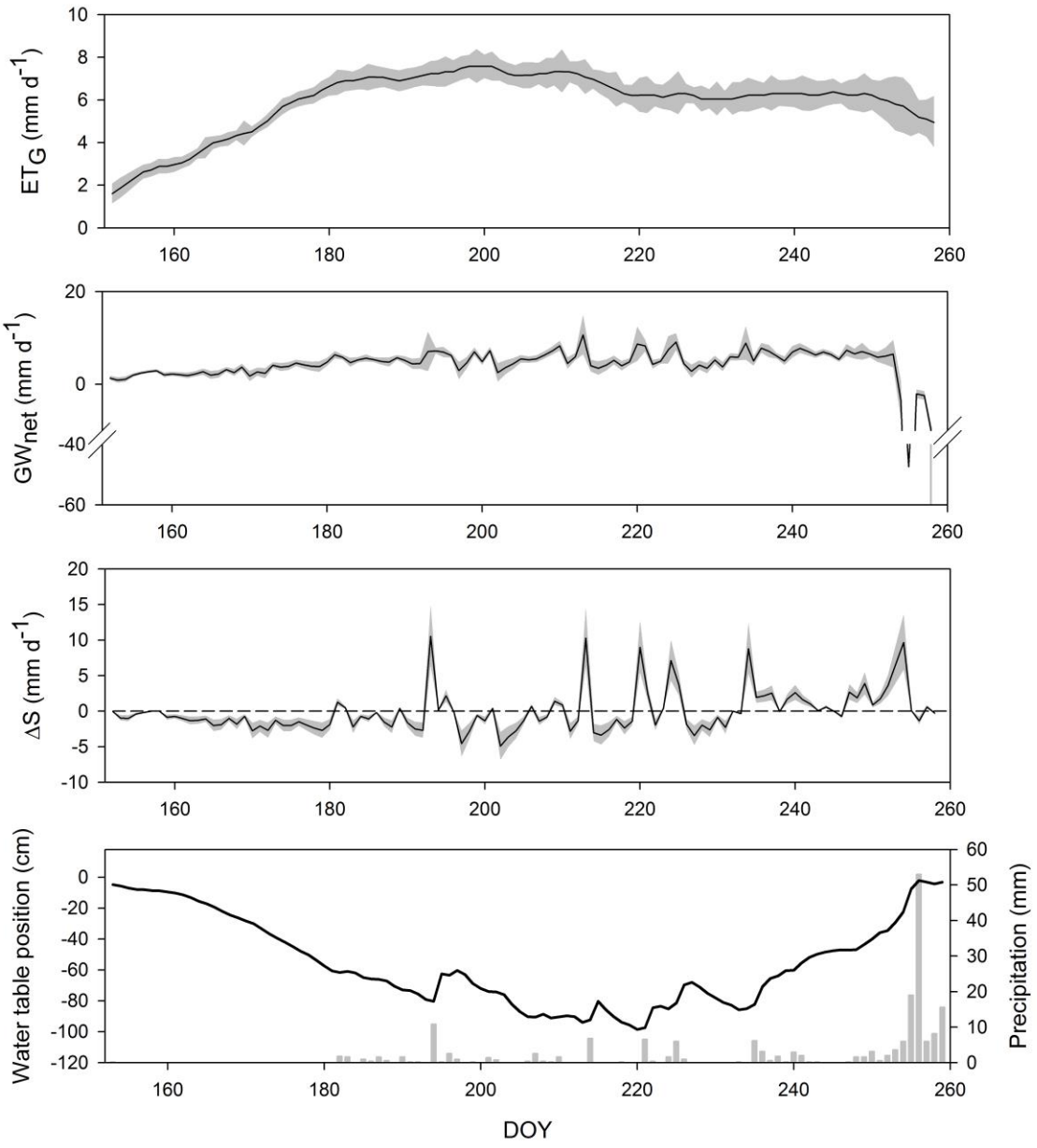

Figure 3.6d. Daily growing season water budget components for Sand Lake Fen in 2013. For ET_G, GW_{net}, and ΔS, solid black lines represent posterior mean estimates for daily fluxes and the shaded regions represent the 95% credible limits. Mean daily water table position is represented by a solid black line and daily total precipitation is represented by grey bars.

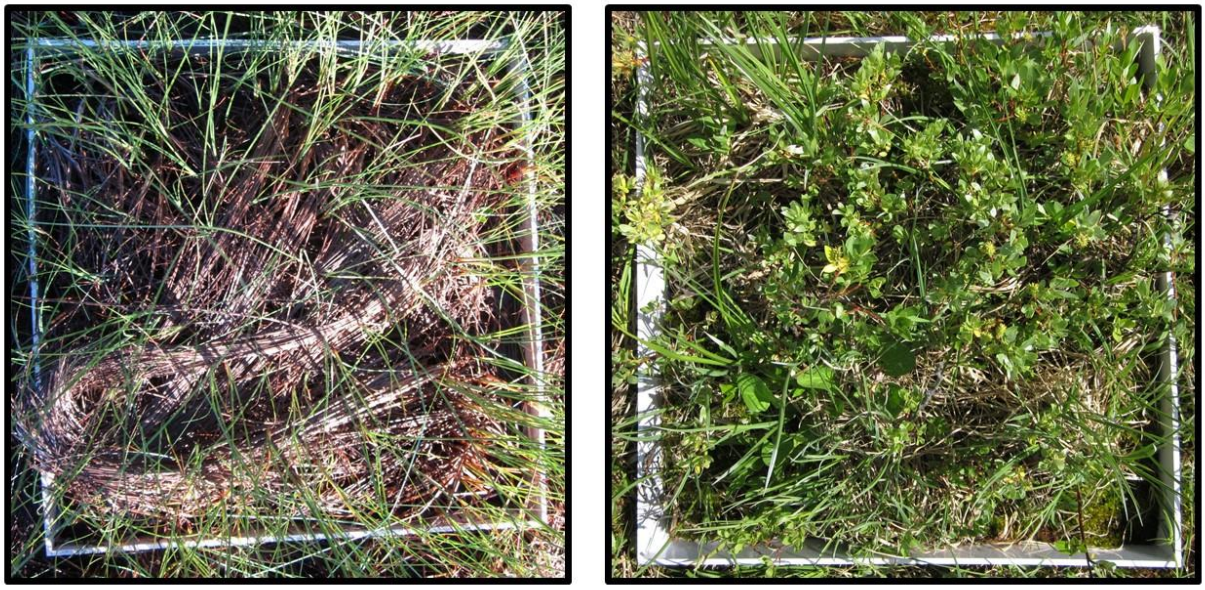

Figure 3.7. Vegetation cover at Anglica Fen (left) and Sand Lake Fen (right).

References

Balwinder-Singh, Eberbach PL, Humphreys E, Kukal SS (2011) The effect of rice straw mulch on evapotranspiration, transpiration and soil evaporation of irrigated wheat in Punjab, India. *Agricultural Water Management*, **98**, 1847–1855.

Bonfils CJW, Phillips TJ, Lawrence DM, Cameron-Smith P, Riley WJ, Subin ZM (2012) On the influence of shrub height and expansion on northern high latitude climate. *Environmental Research Letters*, **7**, 015503.

Bridgham SD, Pastor J, Updegraff K, Malterer TJ, Harth C, Chen J (1999) Ecosystem Control over Temperature and Energy Flux in Northern Peatlands. *Ecological Applications*, **9**, 1345–1358.

Carlson Mazur ML, Wiley MJ, Wilcox D a. (2013) Estimating evapotranspiration and groundwater flow from water-table fluctuations for a general wetland scenario. *Ecohydrology*, n/a–n/a.

Chimner RA, Cooper DJ (2003a) Influence of water table levels on CO2 emissions in a Colorado subalpine fen: an in situ microcosm study. *Soil Biology and Biochemistry*, **35**, 345–351.

Chimner RA, Cooper DJ (2003b) Carbon dynamics of pristine and hydrologically modified fens in the southern Rocky Mountains. *Canadian Journal of Botany*, **81**, 477–491.

Chimner R a., Lemly JM, Cooper DJ (2010) Mountain Fen Distribution, Types and Restoration Priorities, San Juan Mountains, Colorado, USA. *Wetlands*, **30**, 763–771.

Christensen NS, Lettenmaier DP (2007) A multimodel ensemble approach to assessment of climate change impacts on the hydrology and water resources of the Colorado River Basin. *Hydrology and Earth System Sciences*, **11**, 1417–1434.

Clow DW (2010) Changes in the Timing of Snowmelt and Streamflow in Colorado: A Response to Recent Warming. *Journal of Climate*, **23**, 2293–2306.

Cooper DJ, Andrus RE (1994) Patterns of vegetation and water chemistry in peatlands of the west-central Wind River Range, Wyoming, U.S.A. *Canadian Journal of Botany*, **72**, 1586–1597.

Cristea NC, Kampf SK, Burges SJ, Asce F (2013) Revised Coefficients for Priestley-Taylor and Makkink-Hansen Equations for Estimating Daily Reference Evapotranspiration. 1289–1300.

Dwire KA, Kauffman JB, Baham JE (2006) Plant species distribution in relation to water-table depth and soil redox potential in montane riparian meadows. *Wetlands*, **26**, 131–146.

Fahle M, Dietrich O (2014) Estimation of evapotranspiration using diurnal groundwater level fluctuations: Comparison of different approaches with groundwater lysimeter data. *Water Resources Research*, **50**, 273–286.

Gauer P (2001) Numerical modeling of blowing and drifting snow in Alpine terrain. *Journal of Glaciology*, **47**, 97–110.

Gorham E (1991) Northern peatlands: Role in the carbon cycle and and probable response to climatic warming. *Ecological Applications*, **1**, 182–195.

Hamlet AF, Mote PW, Clark MP, Lettenmaier DP (2005) Effects of temperature and precipitation variability on snowpack trends in the sestern United States. *Journal of Climate*, **18**, 4545–4561.

Holden J, Burt TP (2002) Infiltration, runoff and sediment production in blanket peat catchments: implications of field rainfall simulation experiments. *Hydrological Processes*, **16**, 2537–2557.

Kellogg DQ, Gold AJ, Groffman PM, Stolt MH, Addy K (2009) Riparian ground-water flow patterns using flownet analysis: Evapotranspiration-induced upwelling and implications for N removal. *Journal of the American Water Resources Council*, **44**, 1024–1034.

Kløve B, Ala-Aho P, Bertrand G et al. (2014) Climate change impacts on groundwater and dependent ecosystems. *Journal of Hydrology*, **518**, 250–266.

Lautz LK (2008) Estimating groundwater evapotranspiration rates using diurnal water-table fluctuations in a semi-arid riparian zone. *Hydrogeology Journal*, **16**, 483–497.

Loheide SP (2008) A method for estimating subdaily evapotranspiration of shallow groundwater using diurnal water table fluctuations. *Ecohydrology*, **1**, 59–66.

Loheide SP, Butler JJ, Gorelick SM (2005) Estimation of groundwater consumption by phreatophytes using diurnal water table fluctuations: A saturated-unsaturated flow assessment. *Water Resources Research*, **41**, n/a–n/a.

Mahmood TH, Vivoni ER (2014) Forest ecohydrological response to bimodal precipitation during contrasting winter to summer transitions. *Ecohydrology*, **7**, 998–1013.

McCreight JL, Small EE (2014) Modeling bulk density and snow water equivalent using daily snow depth observations. *The Cryosphere*, **8**, 521–536.

Mukherjee a., Kundu M, Sarkar S (2010) Role of irrigation and mulch on yield, evapotranspiration rate and water use pattern of tomato (Lycopersicon esculentum L.). *Agricultural Water Management*, **98**, 182–189.

Parajka J, Haas P, Kirnbauer R, Jansa J, Blöschl G (2012) Potential of time-lapse photography of snow for hydrological purposes at the small catchment scale. *Hydrological Processes*, **26**, 3327–3337.

Parida BR, Buermann W (2014) Snow depth, density, and SWE estimates derived from GPS reflection data: Validation in the western U. S. *Geophysical Research Letters*, **GL060495**, 5476–5483.

Patterson L, Cooper DJ (2007) The use of hydrologic and ecological indicators for the restoration of drainage ditches and water diversions in a mountain fen, Cascade Range, California. *Wetlands*, **27**, 290–304.

Regonda SK, Rajagopalan B, Clark M, Pitlick J (2004) Seasonal Cycle Shifts in Hydroclimatology over the Western United States. *Journal of Climate*, **18**, 372–384.

Riutta T, Laine J, Tuittila E-S (2007) Sensitivity of CO2 Exchange of Fen Ecosystem Components to Water Level Variation. *Ecosystems*, **10**, 718–733.

Rood SB, Pan J, Gill KM, Franks CG, Samuelson GM, Shepherd A (2008) Declining summer flows of Rocky Mountain rivers: Changing seasonal hydrology and probable impacts on floodplain forests. *Journal of Hydrology*, **349**, 397–410.

Rosenberry DO, Winter TC (1997) Dynamics of water-table fluctuations in an upland between two prairie-pothole wetlands in North Dakota. *Journal of Hydrology*, **191**, 266–289.

Rosenberry DO, Stannard DI, Winter TC, Martinez ML (2004) Comparison of 13 equations for determining evapotranspiration from a prairie wetland, Cottonwood Lake Area, North Dakota, USA. *Wetlands*, **24**, 483–497.

Roulet NT, Moore TR, Bubier JL, Lafleur PM (1992) Northern fens: methane and climate change. *Tellus B*, **44**, 100–105.

Schimelpfenig DW, Cooper DJ, Chimner R a. (2013) Effectiveness of Ditch Blockage for Restoring Hydrologic and Soil Processes in Mountain Peatlands. *Restoration Ecology*, **22**, 257-265.

Stein ED, Mattson M, Fetscher a. E, Halama KJ (2004) Influence of geologic setting on slope wetland hydrodynamics. *Wetlands*, **24**, 244–260.

Thompson DK, Benscoter BW, Waddington JM (2014) Water balance of a burned and unburned forested boreal peatland. *Hydrological Processes*, **28**, 5954–5964.

Winter TC (1999) Relation of streams , lakes , and wetlands to groundwater flow systems. *Hydrogeology Journal*, **7**, 28–45.

Wolfe BE, Weishampel P a., Klironomos JN (2006) Arbuscular mycorrhizal fungi and water table affect wetland plant community composition. *Journal of Ecology*, **94**, 905–914.

Woods SW, Macdonald LH, Westbrook CJ (2006) Hydrologic interactions between an alluvial fan and a slope wetland in the central Rocky Mountains, USA. *Wetlands*, **26**, 230–243.

Wu J, Roulet NT, Sagerfors J, Nilsson MB (2013) Simulation of six years of carbon fluxes for a sedge-dominated oligotrophic minerogenic peatland in Northern Sweden using the McGill Wetland Model (MWM). *Journal of Geophysical Research: Biogeosciences*, **118**, 795–807.

4 Simulating water table dynamics and ecosystem-atmosphere carbon exchange under future climate scenarios in a montane fen

4.1 Introduction

Climate change is expected to have significant impacts on terrestrial ecosystem dynamics and hydrological cycles. Ecosystems characterized by cold climates such as those found in mountain environments are particularly susceptible, as warmer temperatures cause earlier melting of snow in the spring, leading to decreased productivity due to drought stress later in the summer (Ernakovich *et al.*, 2014; Parida & Buermann, 2014). In addition, warming of air to temperatures above freezing changes the phase of precipitation from snow to rain, reducing annual snow accumulation, especially near elevations that represent the lower limit of snow persistence in the western US (Christensen & Lettenmaier, 2007; Ashfaq *et al.*, 2013), further altering the timing and magnitude growing season hydrological fluxes (Rood *et al.*, 2008; Godsey *et al.*, 2014).

Of the ecosystems found in cold regions likely to be affected by a changing climate, peatlands are of particular concern, due to their dependence on a perennially high water table and their role in mediating fluxes of greenhouse gases (GHG) (Belyea 2009). Water tables (WT) near the soil surface in peatlands favor the sequestration of carbon dioxide (CO_2), which has led these ecosystems to accumulate approximately 1/3 of the terrestrial carbon (C) on earth via organic soil formation (Gorham, 1991), ultimately causing them to have a net global cooling effect over the past 8,000 to 11,000 years (Frolking & Roulet, 2007). However, near-surface WTs also create reduced soil environments, and are responsible for peatlands being among the largest natural sources of atmospheric methane (CH_4) (Bridgham *et al.*, 2013), a GHG with a recently

revised global warming potential (GWP) approximately 34 times more potent than CO_2 at a century time scale (Myhre *et al*. 2013).

Climate change has the potential to alter peatland GHG dynamics indirectly by driving changes in hydrological cycles that affect WT position (Moore *et al.*, 1998). Water table manipulation experiments have shown that peatland ecosystem respiration (ER) increased when WT position declined (Moore & Knowles, 1989; Chimner & Cooper, 2003a). If WT declines in peatlands occur as a result of climate-driven changes in hydrological cycles, increases in ER can cause net ecosystem production (NEP) to decline, shifting them from CO_2 sinks to sources (Riutta *et al.*, 2007a; Wu *et al.*, 2013). In addition, CH_4 emissions tend to decline with WT in peatlands, as greater proportions of the peat profile become exposed to aerobic conditions (Turetsky *et al.*, 2008; Gong *et al.*, 2013). Further, peatland CH_4 emissions can be positively correlated with NEP (Whiting & Chanton, 1993; Bellisario *et al.*, 1999) as methanogen substrate availability increases with NEP, as well as the potential for plant-mediated transport of CH_4, particularly in fens (Turetsky *et al.*, 2014). Future increases in air temperature also have the potential to impact GHG dynamics in peatlands directly, by increasing the metabolic rates of organisms that mediated fluxes of CO_2 and CH_4 (Sullivan *et al.*, 2007; Turetsky *et al.*, 2008).

Peatland ecosystems occur at high elevations in the Rocky Mountains of the western US, and have been sequestering atmospheric C for many millennia (Chimner *et al.*, 2002). In the San Juan Mountains of southwest Colorado, these ecosystems occur from approximately 2,600 to 3,700 m in elevation, and contain plant species characteristic of peatlands in boreal regions of North America and Europe (Chimner *et al.*, 2010). The majority of precipitation falls as snow in the San Juan Mountains and the snowpack typically persists through early summer at high

elevations (Landry *et al.*, 2014). The dominant growing season precipitation source is rainfall driven by the late summer North American monsoon (Costigan *et al.*, 2000).

Because a warmer climate is likely to have the strongest influence on mountain snowpacks at lower elevations in the Rocky Mountains (Christensen & Lettenmaier, 2007), it is likely that impacts on fen hydrology will be most pronounced to low elevation fens. Earlier snowmelt in low elevation fens will likely impact C budgets (Aurela, 2004), and extend the period of time between the onset of the snow-free season and the beginning of the monsoon season.

In this study, I modeled changes in hydrological cycles and subsequently peatland atmosphere C exchange at a low elevation fen in the San Juan Mountains. The modeling effort included two phases. First I modeled changes in hydrological dynamics based on increasing air temperatures to predict WT under two future climate scenarios. Second, using the predicted WT dynamics along with increased air temperature, I modeled potential future growing season CO_2 and CH_4 budgets.

4.2 Methods

The study took place in a homogenous stand of *Carex lasiocarpa* at Anglica Fen, a basin fen surrounded by bedrock in the San Juan Mountains of southwestern Colorado at an elevation of approximately 2,700 m. The overall modeling effort was composed of two main components, a hydrological model that estimated WT position during the winter and spring (November 5th to April 5th), and a biogeochemical model that estimated ecosystem CO_2 and CH_4 fluxes during the growing season (May 28th to September 19th). Both the hydrological and biogeochemical models were run under 3 scenarios. Each model was run using field data collected in 2011-12, as well as two additional model runs, performed under potential future climate scenarios for the Rocky

Mountains, in which air temperature was increased by 2 and 4 °C, respectively (Christensen & Lettenmaier, 2007; Liu *et al.*, 2013).

Hydrological modeling during the snow-covered season

The primary focus of the hydrological model was to simulate changes in winter precipitation and snow accumulation, and their subsequent impact on WT dynamics preceding the growing season under a future climate. I used two approaches for modeling changes in the snow pack. First, using mean daily air temperature, daily precipitation was partitioned into rain or snow using a 6th order polynomial function, calibrated for the western US, to calculate the probability of snow for air temperatures between 0.45 and 5.97 °C (Auer 1974, Fassnacht and Soulis 2002) (Equation 1).

$$\boldsymbol{P_{snow}(T) = a_1 T_a^6 + a_2 T_a^5 + a_3 T_a^4 + a_4 T_a^3 + a_5 T_a^2 + a_6 T_a + b} \quad \textbf{(1)}$$

In Equation 1, P_{snow} is the probability of snow, and a_1 through a_6 and b represent regression coefficients (Table 4.1). This mixed precipitation curve splits total precipitation for a given time step into snow and/or rain (Fassnacht and Soulis 2002). The fraction of daily precipitation falling as snow was calculated by multiply the total amount by P_{snow}, and the fraction falling as rain was determined as the remainder. It was assumed that all precipitation fell as snow at daily mean air temperatures below 0.45 °C, and that all precipitation fell as rain above 5.97 °C.

Once precipitation was partitioned into rain and snow, it was used to run a snowpack accumulation and melt model that predicted SWE on a daily time step, incorporating elements of

a temperature-index snow model (TIM) (Bormann *et al.*, 2014) that uses the snowmelt parameterization scheme of Rango and Martinec (1995). Daily melt potential was calculated using Equation 2.

$$\boldsymbol{Mp = MF\ (T_{mean} - T_{ref})} \quad \textbf{(2)}$$

In Equation 2, *Mp* represents snowmelt potential in cm d^{-1}, *MF* represents a melt parameter in cm $°C^{-1}$ d^{-1}, T_{mean} represents daily mean air temperature in °C, and T_{ref} which represents the temperature above which melting occurs (set to 0°C in the study). Because *MF* varies depending on snow density, it was calculated on a daily basis using Equation 3.

$$\boldsymbol{MF = k * \frac{\rho_s}{\rho_w}} \quad \textbf{(3)}$$

In Equation 3, *k* is set to 1.1 cm $°C^{-1}$ d^{-1}, according to Rango and Martinec (1995). Snow density in g cm^{-3} is represented by ρ_s, and ρ_w represents the density of water, which is set at 1 g cm^{-3}. As ρ_s varies throughout the snow-covered season, I used an on-site estimate of ρ_s along with a snow densification rate of 0.001 g cm^{-3} d^{-1} (Bormann *et al.*, 2013) to estimate daily ρ_s throughout the snow-covered period. A federal sampler was used to conduct a snow survey at the site on March 14th, 2012 to estimate ρ_s (μ = 0.40 g cm^{-3}, σ = 0.033 g cm^{-3}, n = 13). The mean ρ_s measured during the snow survey was used for March 14th, and ρ_s for the remainder of the snow covered season (before and after March 14th) were calculated using the snow densification rate.

Once developed, the precipitation and snowpack models were used to predict daily WT position during the snow-covered period, starting with an initial WT position of -2.6 cm

(negative WT is below the peat surface, positive WT is above) observed on November 4th 2011. On each day, precipitation that fell as rain was available to recharge groundwater and raise WT, while daily precipitation falling as snow accumulated as snowpack. On days where *Mp* was > 0, melt water was available for groundwater recharge in the same way as precipitation falling as rain, otherwise snow accumulated above the WT.

Water table position was measured throughout the snow covered season using an In-Situ Rugged Troll (Fort Collins, CO) down-well logging pressure transducer and used to evaluate the snow covered season model. A bias in WT position resulting from the influence of snowpack pressure was observed, in which WT position increased 0.5 cm for every 1 cm of SWE (R^2 = 0.98), so a regression of this bias was used to correct WT position during the snow covered period.

Initially, the model was run using daily mean air temperature and precipitation from the Cascade #2 SNOTEL site, approximately 1 km north of Anglica Fen, for the snow-covered period during the water year of 2012, from November 5th, 2011 to April 5th, 2012. Details on the Cascade #2 SNOTEL site can be found in Chapter 2. Additional model runs were performed to simulate changes in snow-cover season WT position under two possible climate change scenarios for the Rocky Mountains, by increasing air temperature by 2 and 4 °C (Christensen & Lettenmaier, 2007; Liu *et al.*, 2013).

A snowpack persisted throughout most of the snow-covered period, from November 5th to April 5th during the 2012 water year. However, under the climate change scenarios, warmer air temperatures increases daily *Mp*, such that longer and more frequent snow free periods existed during winter, with WT positions above or just below the peat surface. Following snow melt in 2012, WT declined at a rate 0.4 cm d^{-1} from April 6th to June 7th (R^2 = 0.97) due to evaporation,

which spanned a range of mean daily air temperatures from -2.3 to 16.5 °C. This rate of evaporation was incorporated into model runs for days with no snow cover. Equation 4 represents the winter water table model.

$$\boldsymbol{\Delta WT\ position = rainfall + snowmelt - evaporation} \quad \textbf{(4)}$$

Water table position following the snow-covered season

From April 6th to September 19th, hourly WT positions were determined, and used to model ER during the growing season. Increased air temperature in the climate change scenarios had the potential to increase overall evapotranspiration losses from the WT (ET_G). However, using the ET_G model from Chapter 2, ET_G losses from groundwater only increased by an average of less than 0.05 mm d^{-1}, or 3.3 to 5.6 mm per growing season for the +2°C and +4°C scenarios, respectively. Therefore, starting on April 6th, modeled WT for all three model runs were calculated starting with the modeled WT position on April 5th and using observed hourly changes in position from that point forward. This allowed similar changes in WT position in response to summer precipitation events as was observed in 2012, albeit at different depths due to changes in snow-covered season WT dynamics.

Gaseous C flux measurements

CO_2 and CH_4 efflux were measured roughly biweekly during the snow-free season of 2011 and monthly in 2012 using a dynamic closed soil chamber technique. Three ABS plastic collars, 60 cm x 60 cm, inserted approximately 5 cm into the soil, were used as the base for a 2.16 $x10^5$ cm^3 cubic gas flux chamber. See Chapter 1 for a detailed description of all CO_2 flux

measurements. CH_4 efflux rates were determined using the chamber with a light-proof cover, collecting four midday gas samples at 10-minute intervals, over 30 minutes. At each sampling interval 30 mL of chamber gas was sampled using a 50-mL syringe, and transferred to a 20-mL evacuated vial. A Los Gatos methane/carbon dioxide/water vapor analyzer (Mountain View, CA) was used to analyze CH_4 concentrations in each vial. A field blank composed of N_2 gas and CH_4 standard (5.03 ppm) were used to ensure no changes in concentration occurred in CH_4 samples between field sampling and laboratory analysis. CH_4 flux rates were calculated as the slope of the linear regression between concentration and time (Turetsky *et al.*, 2008).

Modeling growing season CO_2 exchange and CH_4 efflux

Chapter 1 describes the CO_2 flux models (gross primary production (GPP), ER, and NEP) in detail, which were used to estimate growing season NEP in this study with several changes. WT position data collected in the growing season of 2012, as well as simulated WT position data for the +2°C and +4°C climate change scenarios were used as input data for the ER model for the three runs. Similarly, 2012 hourly air temperature was used for the 2012 growing season model run, while 2 and 4 °C were added to each hourly measurement for the two climate change scenarios. Running averages of daily air temperature (RAV) were also increased by 2 and 4 °C for the GPP and ER models in their respective climate change scenarios.

A simple linear regression was used to model CH_4 efflux during the growing season as a function of NEP (Equation 5).

$$\boldsymbol{CH_4 = NEP * \beta_0 + \beta_1} \quad \textbf{(5)}$$

In estimating model parameters, mean midday NEP and CH_4 fluxes for all three soil collars were used for each sampling day. As with the CO_2 flux models described in Chapter 1, the CH_4 model in this study was fit to the measured data using Bayesian methods in R statistical software. Model parameters were estimated using Markov chain Monte Carlo (MCMC) analysis in the *rjags* package for R (Plummer, 2011). A total of 100,000 iterations were used with 3 MCMC chains, after a burn-in of 60,000 iterations. Vague normal priors were used for all model parameters. Equation 6 represent the likelihood functions for the observed CH_4 ($CH_{4_i}^{obs}$) as a function of NEP.

$$\boldsymbol{CH_{4_i}^{obs} \sim Normal(\mu CH_{4_i}, \sigma_{procCH_4})} \quad \textbf{(6)}$$

In Equation 5, μCH_{4_i} represents the predicted values of CH_4 and σCH_{4_i} represents the process variance associated with those predictions.

Growing season estimates of NEP, CH_4 efflux, and the combined growing season GWP of CO_2 and CH_4 (in CO_2 equivalents) were determined for all three scenarios, as the sum of hourly flux estimates. A total of 6,000 iterations were used with 3 MCMC chains, after a burn-in of 3,000 iterations to estimate growing season fluxes. I used a Bayesian t-test alternative to compare mean growing season flux estimates among scenarios. The BEST package for R uses Bayesian estimation to determine the 95% highest density interval (HDI) of the difference between two means (Kruschke 2013). Differences between growing season flux estimates were determined to be credible if their 95% HDI did not overlap zero. A random sampling of 5,000 iterations, from the total 18,000 iterations for each growing season flux estimate, were used as inputs for each of the two means being compared using BEST.

4.3 Results

Snowpack and water table dynamics during the snow-covered season

Overall, modeled daily SWE for the 2012 water year accurately captured changes in daily SWE observed at the Cascade #2 SNOTEL site (Figure 4.1). Additionally, modeled peak SWE (27 cm) closely matched measured peak SWE (26 cm) on March 3rd, 2012. Peak SWE under the +2°C scenario declined by almost half, to 15 cm. Similarly, peak SWE under the +4°C scenario was almost half that of the +2°C scenario, at 8 cm. Snow melt during the modeling period was progressively greater for the future climate scenarios. Seven snow-free days occurred towards the end of the modeling period during the 2011-12 model run. Snow-free periods occurred early during the modeling period for both climate change scenarios and persisted for longer, with 37 and 68 snow-free days for the +2°C and +4°C scenarios (Figure 4.2).

Modeled daily WT position matched observed changes in WT well ($R^2 = 0.94$) through the snow-covered season (Figure 4.3). Under the 2011-12 model run, WT position remained stable during the snow-covered season, due to relatively little groundwater recharge derived from melting snow. Fluctuations in WT were more frequent and of greater magnitude under the climate change scenarios, however, due to more frequent and substantial snow melt events throughout the modeling period (Figure 4.2). Modeled WT on April 5th, 2012 was within one cm of the observed WT for that date, at 27 cm above the peat surface in 2011-12. Due to a greater frequency of snow-free days during the modeling period, both climate change scenarios had a greater evaporative loss from the WT, resulting in April 5th WT positions of 17 and 8 cm above the peat surface for the +2°C and +4°C scenarios, respectively, which led to lower WT during the growing season under these scenarios (Figure 4.4).

Growing season ecosystem-atmosphere C exchange

Measured NEP ranged from -0.20 to 2.21 g CO_2 m^{-2} hr^{-1}, and measured CH_4 efflux ranged from 0.65 to 21 mg CH_4 m^{-2} hr^{-1}. Modeled estimates of NEP during the 2012 growing season indicate that the site acted as a net source of CO_2 during 2012, with a mean flux rate of -95 g CO_2 m^{-2} gs^{-1}, while modeled mean CH_4 efflux for the same growing season was 10.2 g m^{-2} gs^{-1}. Mean measured CH_4 efflux was positive correlated with mean measured NEP (Figure 4.5, Table 4.2). Credible differences were found between mean growing season flux estimates between each scenario for NEP, CH_4 efflux, and combined emissions (Figure 4.6). Mean growing season CH_4 efflux rates decreased by 10% under the +2°C climate scenario and by 21% under the +4°C scenario. Compared to the 2012 estimate, mean growing season NEP decreased by approximately 81% under the +2°C climate scenario and approximately 200% in under the +4°C scenario**.** Net combined emissions of CO_2 and CH_4 increased under the warming scenarios by 14 under the +2°C climate scenario and 28% under the +42°C climate scenario.

4.4 Discussion

Water table dynamics under a future climate

The snow-covered season hydrological model simulated realistic changes in hydrological cycles under a warmer future climate. Future climate projections show an increase in air temperature for the Rocky Mountains (Christensen & Lettenmaier, 2007; Liu *et al.,* 2013). However, current climate models suggest that annual precipitation totals will remain highly variable from year to year, with no projected trend of increasing or decreasing precipitation (Harding *et al.,* 2012). The hydrological simulations used in this study present an appropriate method for identifying possible future changes in fen hydrological cycles using changes in WT dynamics that could result from increased air temperatures with identical precipitation inputs.

Modeled daily changes in WT position followed observed changes closely, and only lagged observed rises in WT slightly during the snowmelt period. Throughout the modeling period, the net flow of groundwater (inflow – outflow) was negligible, evident by the lack of increase or decrease in WT position during the 2012 snow-covered season, and the results of 2012 growing season water budget from Chapter 2. The +2 °C and +4 °C climate change scenarios lead to a substantially lower WT position throughout the growing season, 11 to 18 cm lower than measured in 2012. Similar projected WT declines, ranging from 14 to 22 cm under future climate conditions, have been projected for higher latitude fens in North America (Roulet *et al.*, 1992).

In this study, the lower growing season WT positions under the warming scenarios were primarily caused by increased loss of water via evaporation, due to lower peak SWE and longer periods of snow-free conditions during the winter and early spring. Similarly, declines in summer streamflow have been attributed to reductions in SWE over recent decades (Rood *et al.*, 2008; Clow, 2010) and predicted to continue in the future as more winter precipitation falls as rain rather than snow (Godsey *et al.*, 2014), in mountain regions of the western US.

Future ecosystem-atmosphere C exchange and implications for climate feedbacks

Modeled NEP was negative for the 2012 growing season at Anglica Fen. Increased ER under the warming scenarios, due to higher air temperatures and lower WT, resulted in additional reductions of NEP. The site was a source of CH_4 under all three climate scenarios, and growing season efflux decreased under the warming climate scenarios. The measured and modeled fluxes of CO_2 and CH_4 in 2012 are similar to previously reported rates for peatlands in the Rocky Mountains (Wickland *et al.*, 2001; Chimner & Cooper, 2003b).

Although the CH_4 model used in this study is quite simplistic, and only uses NEP as a predictor variable, the correlation between CH_4 and NEP has been observed across a wide range of wetland types (Whiting & Chanton, 1993; Bellisario *et al.*, 1999; Joabsson & Christensen, 2001). Increases in temperature drive increases in CH_4 efflux rates, while declines in WT position can lead to decreased CH_4 efflux rates (Moore & Knowles, 1989; Turetsky *et al.*, 2008, 2014). The NEP model used in this study responded to air temperature and WT position in the same way. As air temperature increases, so does ER, and as the WT declines exposing more of the peat profile, it also causes ER to increase, driving changes in NEP. Thus, the important abiotic factors that control wetland CH_4 efflux are also incorporated in the NEP model used in this study.

Several sources of uncertainty exist for predicting future GHG fluxes. Plant community type plays an important role in controlling both CO_2 and CH_4 in wetland ecosystems (Johansson *et al.*, 2006; Riutta *et al.*, 2007b), and future changes in peatland plant community composition are likely as a result of warmer temperatures and lower WT (Weltzin *et al.*, 2003). In addition, the CH_4 efflux model in this study likely underestimated total emissions, as it did not account for ebullition events, which can contribute from 18 – 50% of total CH_4 emissions (Christensen *et al.*, 2003). Despite these shortcomings, this study elucidates how ecosystem-atmosphere C exchange in a sedge-dominated peatland, an ecosystem type of great biogeochemical significance in boreal and mountain regions of the world (Gorham 1991; Belyea 2009; Turetsky et al 2014), will likely respond to a warming climate, providing conservative estimates of GWP under future climate scenarios. Further, the climate change scenarios in this study represent plausible changes in temperature and WT dynamics at Anglica Fen, rather than simply performing a sensitivity analysis on the 2012 model based on WT and air temperature (Wu *et al.*, 2013).

My results show that although decreases in CH_4 efflux are predicted under future climate scenarios for Anglica Fen, the overall GWP of the combined CH_4 and CO_2 fluxes increases. This suggests that despite the potential negative feedback to a warming climate through decreased CH_4 efflux, positive feedback to a changing climate may occur in the future, resulting from the overshadowing effect of more substantial increases in CO_2 efflux. Further, Rocky Mountain fens at similar elevations as Anglica Fen are at risk of accelerated rates of soil loss through decomposition under future climate scenarios.

Table 4.1. Sixth order polynomial mixed precipitation model parameters.

Parameter	Value
a_1	0.0202
a_2	-0.366
a_3	2.0399
a_4	-1.5089
a_5	-15.038
a_6	4.6664
b	100

Table 4.2. Mean parameter estimates for CH_4 model.

	Parameter estimate*
β_0	11.3 (3.9)
β_1	4.0 (2.3)
σ_{proc}	4.5 (1.4)

* Values in parentheses represent standard deviation.

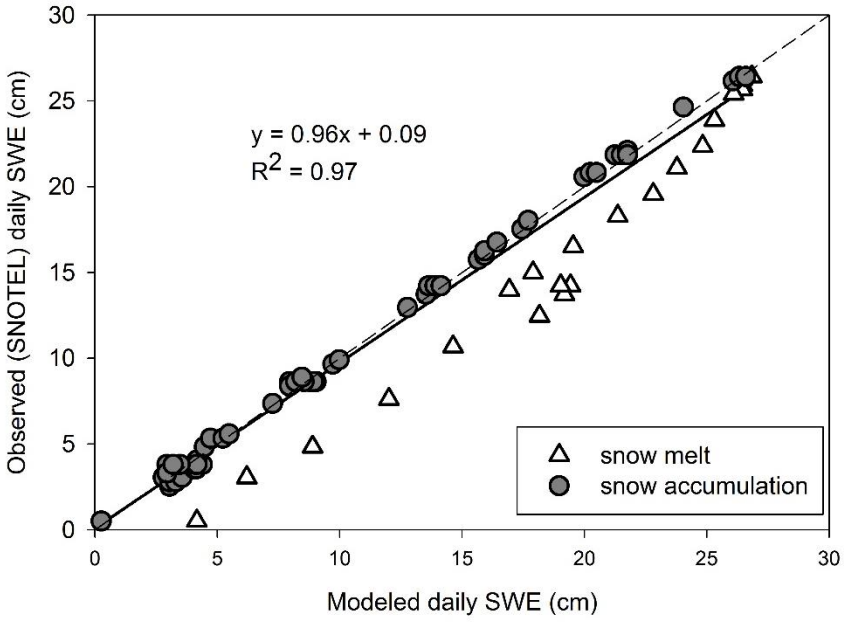

Figure 4.1. Observed daily SWE from the Cascade #2 SNOTEL site versus modeled daily SWE at Anglica Fen. Circles represent daily SWE estimates between onset of snow accumulation and peak SWE, and triangles represent daily SWE estimates between peak SWE and complete melt. The dashed line represents the 1:1 line and the bold line represents the best fit model.

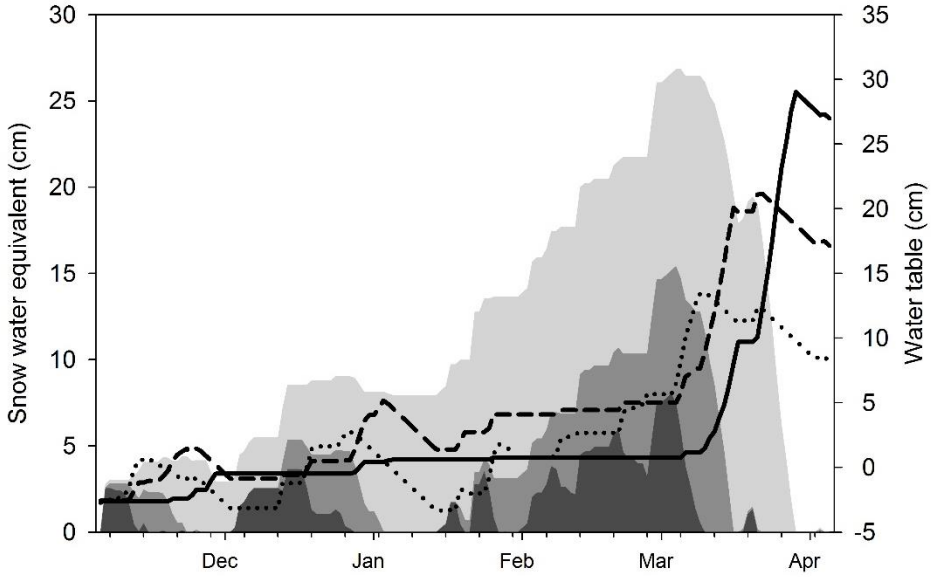

Figure 4.2. Snow water equivalent (SWE) and water table dynamics for all three model runs. Shaded areas represent SWE for the 2012 water year (light grey), +2 °C scenario (medium grey), and +4 °C (dark grey). Lines represent daily WT position for the 2012 water year (solid), +2 °C scenario (dashed), and +4 °C (dotted).

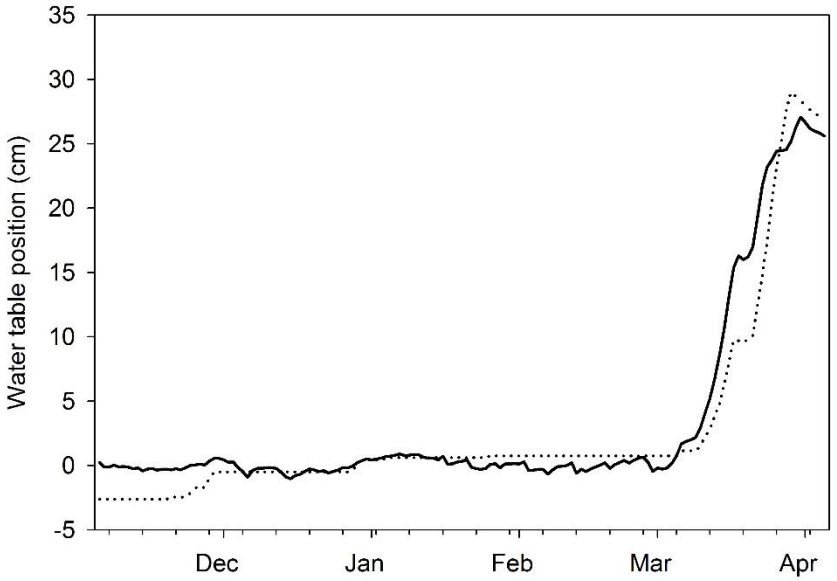

Figure 4.3. Corrected observed water table position (black line) and modeled water table position (dotted line) from November 5th to April 5th during the 2012 snow year.

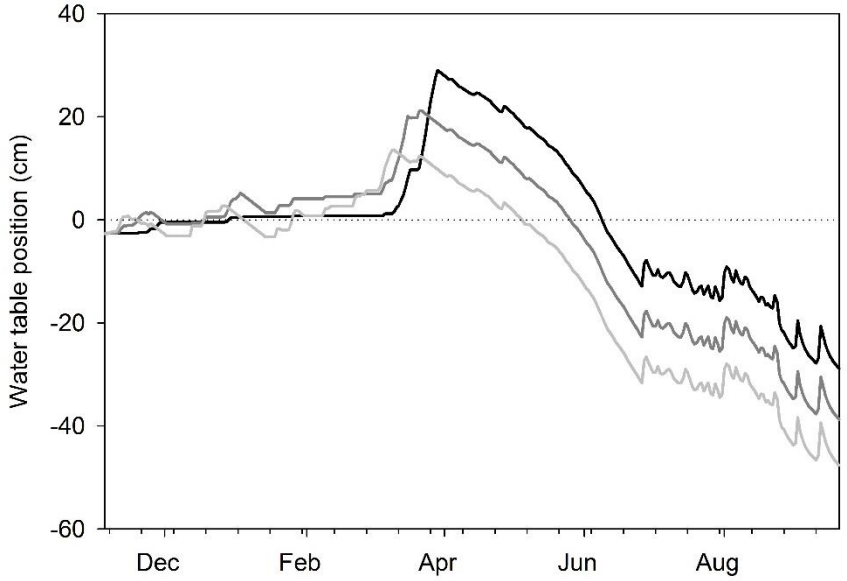

Figure 4.4. Hydrographs for November 5th to September 19th during the 2012 water year (black line), the +2 °C scenario (dark grey line), and the +4 °C scenario (light grey line). Dotted line represents the soil surface.

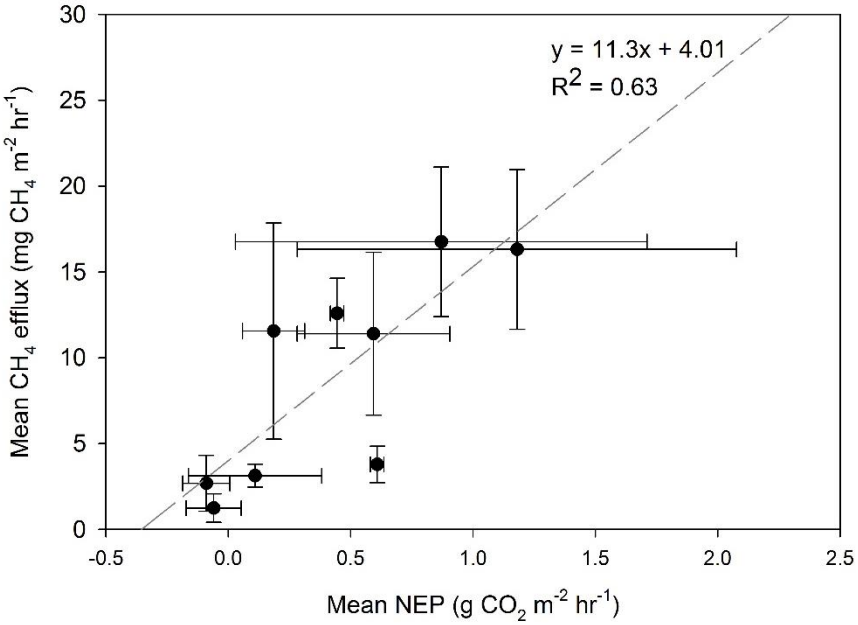

Figure 4.5. Mean measured CH_4 vs mean measured NEP. Error bars represent standard deviation, and the dashed grey line represents the best-fit model.

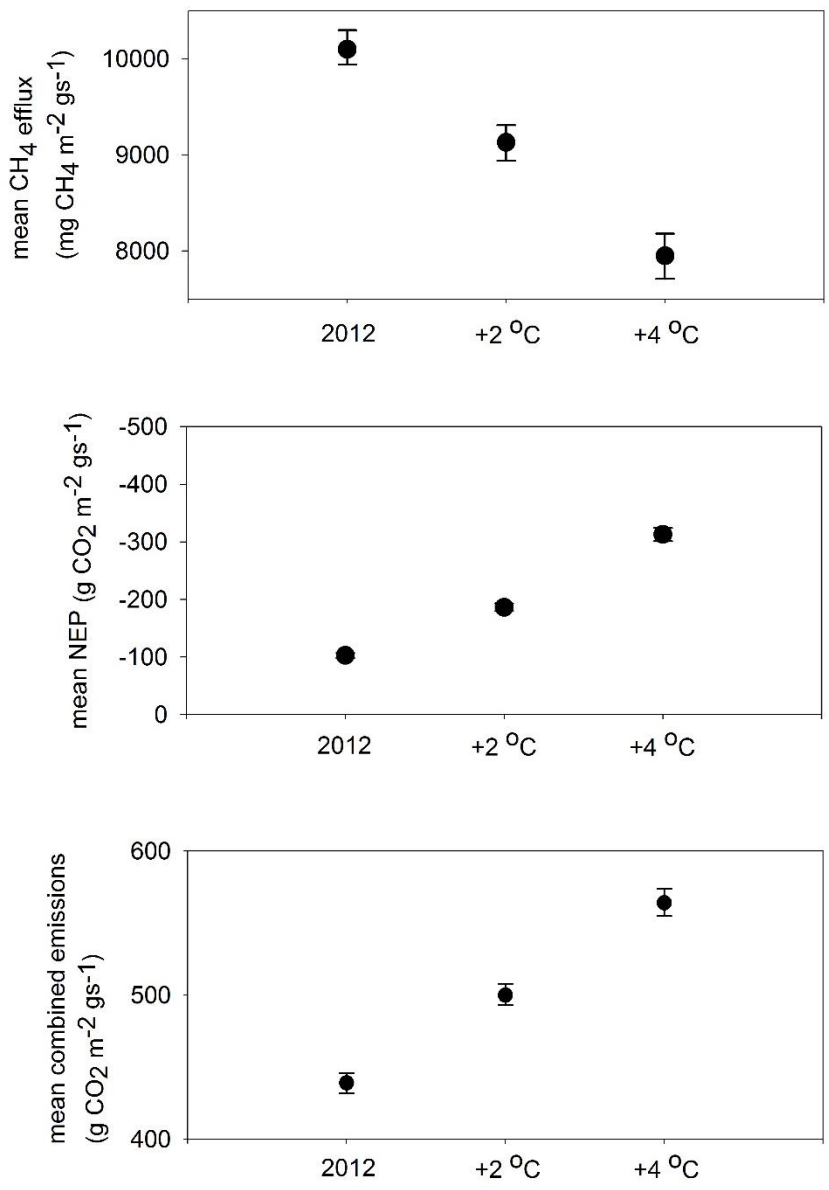

Figure 4.6. Mean estimates for NEP, CH_4, and combined emissions (CO_2 and CH_4) for all three model scenarios. Error bars represent the highest density interval of the mean estimates.

References

Ashfaq M, Ghosh S, Kao S-C et al. (2013) Near-term acceleration of hydroclimatic change in the western U.S. *Journal of Geophysical Research: Atmospheres*, **118**, 10,676–10,693.

Auer, AH (1974) The rain versus snow threshold temperatures. *Weatherwise*, **27**: 67.

Aurela M (2004) The timing of snow melt controls the annual CO_2 balance in a subarctic fen. *Geophysical Research Letters*, **31**, L16119.

Bellisario LM, Bubier JL, Moore TR (1999) Controls on CH_4 emissions from a northern peatland. *Global Biogeochemical* Cycles, **13**, 81–91.

Belyea, LR (2009) Nonlinear dynamics of peatlands and potential feedbacks on the climate system, in Carbon Cycling in Northern Peatlands, *Geophysical Monograph Series*, **184**, edited by A. J. Baird et al., pp. 5–18, AGU, Washington, D. C.

Bormann KJ, Westra S, Evans JP, McCabe MF (2013) Spatial and temporal variability in seasonal snow density. *Journal of Hydrology*, **484**, 63–73.

Bormann KJ, Evans JP, McCabe MF (2014) Constraining snowmelt in a temperature-index model using simulated snow densities. *Journal of Hydrology*, **517**, 652–667.

Bridgham SD, Cadillo-Quiroz H, Keller JK, Zhuang Q (2013) Methane emissions from wetlands: biogeochemical, microbial, and modeling perspectives from local to global scales. *Global change biology*, **19**, 1325–46.

Chimner RA, Cooper DJ (2003a) Influence of water table levels on CO_2 emissions in a Colorado subalpine fen: an in situ microcosm study. *Soil Biology and Biochemistry*, **35**, 345–351.

Chimner RA, Cooper DJ (2003b) Carbon dynamics of pristine and hydrologically modified fens in the southern Rocky Mountains. *Canadian Journal of Botany*, **81**, 477–491.

Chimner RA, Cooper DJ, Parton WJ (2002) Modeling carbon accumulation in Rocky Mountain fens. *Wetlands*, **22**, 100–110.

Chimner RA, Lemly JM, Cooper DJ (2010) Mountain Fen Distribution, Types and Restoration Priorities, San Juan Mountains, Colorado, USA. *Wetlands*, **30**, 763–771.

Christensen NS, Lettenmaier DP (2007) A multimodel ensemble approach to assessment of climate change impacts on the hydrology and water resources of the Colorado River Basin. *Hydrology and Earth System Sciences*, **11**, 1417–1434.

Christensen TR, Panikov N, Mastepanov M et al. (2003) Biotic Controls on CO_2 and CH_4 Exchange in Wetlands: A Closed Environment Study. **64**, 337–354.

Clow DW (2010) Changes in the Timing of Snowmelt and Streamflow in Colorado: A Response to Recent Warming. *Journal of Climate*, **23**, 2293–2306.

Costigan KR, Bossert JE, Langley DL (2000) Atmospheric/hydrologic models for the Rio Grande Basin: Simulations of precipitation variability. *Global and Planetary Change*, **25**, 83–110.

Ernakovich JG, Hopping K a., Berdanier AB, Simpson RT, Kachergis EJ, Steltzer H, Wallenstein MD (2014) Predicted responses of arctic and alpine ecosystems to altered seasonality under climate change. *Global Change Biology*, 3256–3269.

Fassnacht SR, Soulis ED (2002) Implications during transitional periods of improvements to the snow processes in the land surface scheme - hydrological model WATCLASS. *Atmosphere-Ocean*, **40**, 389–403.

Frolking S, Roulet NT (2007) Holocene radiative forcing impact of northern peatland carbon accumulation and methane emissions. *Global Change Biology*, **13**, 1079–1088.

Godsey SE, Kirchner JW, Tague CL (2014) Effects of changes in winter snowpacks on summer low flows: case studies in the Sierra Nevada, California, USA. *Hydrological Processes*, **28**, 5048–5064.

Gong J, Kellomäki S, Wang K, Zhang C, Shurpali N, Martikainen PJ (2013) Modeling CO_2 and CH_4 flux changes in pristine peatlands of Finland under changing climate conditions. *Ecological Modelling*, **263**, 64–80.

Gorham E (1991) Northern peatlands: Role in the carbon cycle and and probable response to climatic warming. *Ecological Applications*, **1**, 182–195.

Harding BL, Wood a. W, Prairie JR (2012) The implications of climate change scenario selection for future streamflow projection in the Upper Colorado River Basin. *Hydrology and Earth System Sciences*, **16**, 3989–4007.

Joabsson A, Christensen TR (2001) Methane emissions from wetlands and their relationship with vascular plants: an Arctic example. *Global Change Biology*, **7**, 919–932.

Johansson T, Malmer N, Crill PM, Friborg T, Akerman JH, Mastepanov M, Christensen TR (2006) Decadal vegetation changes in a northern peatland, greenhouse gas fluxes and net radiative forcing. *Global Change Biology*, **12**, 2352–2369.

Kruschke JK (2013) Bayesian Estimation Supersedes the t Test. *Journal of Experimental Psychology: General*, **142**, 573–603.

Landry CC, Buck KA, Raleigh MS, Clark MP (2014) Mountain system monitoring at Senator Beck Basin, San Juan Mountains, Colorado: A new integrative data source to develop and evaluate models of snow and hydrologic processes. *Water Resources Research*, **WR013711**, 1–16.

Liu Y, L. Goodrick S, A. Stanturf J (2013) Future U.S. wildfire potential trends projected using a dynamically downscaled climate change scenario. *Forest Ecology and Management*, **294**, 120–135.

Moore TR, Knowles R (1989) The influence of water table levels on methane and carbon dioxide emmisions from peatland soils. *Canadian Journal of Soil Science*, **69**, 33–38.

Moore TR, Roulet NT, Waddington JM (1998) Uncertainty in the effect of climatic change on the carbon cycling of Canadian peatlands. *Climate Change*, **40**, 229–245.

Myhre, G., D. Shindell, F.-M. Bréon, et al. (2013) Anthropogenic and Natural Radiative Forcing. In: Climate Change 2013: The Physical Science Basis. Contribution of Working Group I to the Fifth Assessment Report of the Intergovernmental Panel on Climate Change [Stocker, T.F., D. Qin, G.-K. Plattner, et al. (eds.)]. Cambridge University Press, Cambridge, United Kingdom and New York, NY, USA.

Parida BR, Buermann W (2014) Snow depth, density, and SWE estimates derived from GPS reflection data: Validation in the western U. S. *Geophysical Research Letters*, **GL060495**, 5476–5483.

Rango, A, Martinec, J (1995) Revisiting the degree-day method for snowmelt computations. *Journal of the American Water Resources Association*, **31,** 657–669.

Riutta T, Laine J, Tuittila E-S (2007a) Sensitivity of CO_2 Exchange of Fen Ecosystem Components to Water Level Variation. *Ecosystems*, **10**, 718–733.

Riutta T, Laine J, Aurela M et al. (2007b) Spatial variation in plant community functions regulates carbon gas dynamics in a boreal fen ecosystem. *Tellus B*, **59**, 838–852.

Rood SB, Pan J, Gill KM, Franks CG, Samuelson GM, Shepherd A (2008) Declining summer flows of Rocky Mountain rivers: Changing seasonal hydrology and probable impacts on floodplain forests. *Journal of Hydrology*, **349**, 397–410.

Roulet NT, Moore TR, Bubier JL, Lafleur PM (1992) Northern fens: methane and climate change. *Tellus B*, **44**, 100–105.

Sullivan PF, Arens SJT, Chimner RA, Welker JM (2007) Temperature and Microtopography Interact to Control Carbon Cycling in a High Arctic Fen. *Ecosystems*, **11**, 61–76.

Turetsky MR, Treat CC, Waldrop MP, Waddington JM, Harden JW, McGuire a. D (2008) Short-term response of methane fluxes and methanogen activity to water table and soil warming manipulations in an Alaskan peatland. *Journal of Geophysical Research*, **113**, G00A10.

Turetsky MR, Kotowska A, Bubier J et al. (2014) A synthesis of methane emissions from 71 northern, temperate, and subtropical wetlands. *Global Change Biology*, **20**, 2183–97.

Weltzin JF, Bridgham SD, Pastor J, Chen J, Harth C (2003) Potential effects of warming and drying on peatland plant community composition. *Global Change Biology*, **9**, 141–151.

Whiting GJ, Chanton JP (1993) Primary production control of methane emission from wetlands. *Nature*, **364**, 794–795.

Wickland KP, Striegl G, Mast MA, Clow DW (2001) Carbon gas exchange at a southern Rocky Mountain wetland, 1996-1998. *Global Biogeochemical Cycles*, **15**, 321–335.

Wu J, Roulet NT, Sagerfors J, Nilsson MB (2013) Simulation of six years of carbon fluxes for a sedge-dominated oligotrophic minerogenic peatland in Northern Sweden using the McGill Wetland Model (MWM). *Journal of Geophysical Research: Biogeosciences*, **118**, 795–807.

5 Synthesis

My dissertation research questions were as follows 1) How does ecosystem-atmosphere CO_2 exchange vary with elevation and monsoon influence in Rocky Mountain peatlands? 2) How do snowmelt dynamics at high and low elevations and varying monsoon influence affect WT dynamics in fens of the Rocky Mountains? 3) How will mountain fen hydrological dynamics likely change under a future climate, and what will be the likely subsequent impact on ecosystem-atmosphere C exchange?

In Chapter 1, I found that NEP was higher for fens located at high elevations compared to those found at lower elevations. This was reflected in the negative correlation of growing season NEP with air temperature, and positive correlation with water table position, as the high elevation sites had the lowest air temperatures and highest water tables. Differences in net ecosystem production associated directly with varying monsoon influence were less discernable.

In Chapter 2, I found that peak snow water equivalent (SWE) was lower for the low elevation fens, and that the snow-free season occurred approximately one month earlier at these sites compared to the high elevation fens. The earlier onset of snow-free conditions led to steady declines in water table position early in the growing season at the low elevation fens, driven primarily by evapotranspiration. Further, the results of this chapter show that hydrological fluxes during the growing season, including net groundwater flow, precipitation, and evapotranspiration, can vary considerable among Rocky Mountain fens.

In Chapter 3, I coupled an empirical model of ecosystem C flux with a hydrological model, and used the models to elucidate the impacts of climate change on ecosystem processes in a low elevation fen in the San Juan Mountains. I found that under future climate scenarios, more winter precipitation fell as rain, peak snow water equivalent was reduced along with the number

of days which snowpack persisted. These changes in hydrological processes led to lower water tables that persisted through the growing season, and subsequently impacted ecosystem-atmosphere C exchange. Under the future climate scenarios, the overall global warming potential of gaseous C emissions increased as a result of increased ecosystem respiration, despite a decreases in CH_4 emissions. Further, the future climate scenarios suggest that the sustainability of low-elevation mountain fens may be in jeopardy, as losses of C exceed gains through primary production.